Inverse Problems

PAPER

A shape optimization approach for electrical impedance tomography with point measurements

IOP Publishing Inverse Problems
Inverse Problems **36** (2020) 095006 (27pp) https://doi.org/10.1088/1361-6420/ab9f87

A shape optimization approach for electrical impedance tomography with point measurements

Yuri Flores Albuquerque[1], **Antoine Laurain**[1,3] and **Kevin Sturm**[2]

[1] Instituto de Matemática e Estatística, Universidade de São Paulo, Rua do Matão 1010, 05508-090, São Paulo, Brazil
[2] Technische Universität Wien, Institut für Analysis und Scientific Computing, Wiedner Hauptstraße 8-10, 1040 Wien, Austria

E-mail: yuri.falbu@gmail.com, laurain@ime.usp.br and kevin.sturm@asc.tuwien.ac.at

Received 6 December 2019, revised 16 June 2020
Accepted for publication 23 June 2020
Published 1 September 2020

Abstract

Working within the class of piecewise constant conductivities, the inverse problem of electrical impedance tomography can be recast as a shape optimization problem where the discontinuity interface is the unknown. Using Gröger's W^1_p-estimates for mixed boundary value problems, the averaged adjoint method is extended to the case of Banach spaces, which allows one to compute the derivative of shape functionals involving point evaluations. We compute the corresponding distributed expression of the shape derivative and show that it may contain Dirac measures in addition to the usual domain integrals. We use this distributed shape derivative to devise a numerical algorithm, show various numerical results supporting the method, and based on these results we discuss the influence of the point measurements patterns on the quality of the reconstructions.

Keywords: electrical impedance tomography, shape optimization, distributed shape derivative, sharp-interface models, PDE-constrained optimization

(Some figures may appear in colour only in the online journal)

1. Introduction

Electrical impedance tomography (EIT) is a low cost, noninvasive, radiation free and portable imaging modality with various applications in medical imaging, geophysics, civil engineering and nondestructive testing. In particular, it is an active field of research in medical imaging,

[3] Author to whom any correspondence should be addressed.

where devices based on EIT are already used in practice, with applications to lung imaging such as diagnosis of pulmonary embolism [19], monitoring patients undergoing mechanical ventilation, breast imaging, acute cerebral stroke, or cardiac activity monitoring; we refer to the reviews [8, 12] and the references therein. In geophysics a similar imaging technique using direct current, called electrical resistivity tomography (ERT), is used for various applications such as environmental investigation, hydrogeology, archeological and mineral exploration; see [56, 59].

Two mathematical models for EIT have been actively investigated over the last few decades. The *continuum model* has been widely studied in the case where applied currents and voltage measurements are supposed to be known on the entire boundary. This model is closely related to the *Calderón problem*, which has attracted the attention of a large community of mathematicians in the last decades; see [8, 12]. It consists of determining the uniqueness and stability properties of the conductivity reconstruction when the full Dirichlet-to-Neumann map is known, which corresponds, roughly speaking, to the availability of an unlimited quantity of applied currents and their associated boundary measurements.

Despite its usefulness, the continuum model is not realistic for applications, indeed, in the case of medical imaging for instance, it does not take into account the fact that currents are applied through electrodes attached by small patches to the patient, and that voltage measurements are also performed through these electrodes. Therefore, the applied currents and voltage measurements are available only on a subset of the boundary. In the literature, this situation is referred to as *partial measurements* as opposed to *full measurements* for the standard Calderón problem. This leads to the more realistic *electrode model* [62], which also takes into account the electro-chemical reaction occurring at the interface between the electrode and the skin.

As the field of EIT has grown more mature, the awareness of these restrictions has increased also among mathematicians. As a consequence, the study of the continuum model with partial boundary data has attracted much attention in the recent years. Uniqueness results with partial boundary data in dimension $n \geqslant 3$ were obtained in [46], in [49] for $\mathcal{C}^2$-conductivities, and in [51] for $W^{3/2+\delta,2n}$-conductivities with $\delta > 0$. Uniqueness results were extended to conductivities of class $\mathcal{C}^{1,\infty}(\overline{\Omega}) \cap H^{3/2}(\Omega)$ and conductivities in $W^{1,\infty}(\Omega) \cap H^{3/2+\delta}(\Omega)$ with $0 < \delta < 1/2$ arbitrarily small but fixed in [52]. We refer to [48] for a review of theoretical results on the Calderón problem with partial data. Regarding numerical methods, sparsity priors are used to improve the reconstruction using partial data in [26, 27]. D-bar methods in two dimensions were investigated in [5, 38] and resistor networks in [13].

Due to the small size of the electrodes compared to the rest of the boundary in many practical applications, the idea of modelling small electrodes by point electrodes using Dirac measures is appealing from the mathematical standpoint. This point of view has been introduced as a *point electrode model* and justified in [33]; see also [15, 42, 43]. Mathematical models using point measurements are for instance highly relevant for large-scale inverse problems in geophysics such as electrical resistivity tomography or full-waveform inversion where the dimensions of the electrodes or receivers are several orders of magnitude smaller than the dimensions of the physical domain of the model; see [59, 67].

The problem of reconstructing conductivities presenting sharp interfaces in EIT, also known as the inclusion detection problem, has attracted significant interest in the last three decades, starting from the pioneering works [24, 25]. Several numerical methods have been developed for reconstructing discontinuous conductivities including the factorization method introduced in [14, 50]; see also the review [34], monotonicity-based shape reconstructions [28, 35, 36], the enclosure method for reconstructing the convex hull of a set of inclusions [44, 45], the MUSIC algorithm for determining the locations of small inclusions [7], a nonlinear integral equation method [22], and topological derivative-based methods [6, 11, 40, 41]. Shape optimization

techniques, which are the basis of the present paper, have also been employed to tackle this problem: based on level set methods [16, 54], for a polygonal partition of the domain [9], using second-order shape sensitivity [3], and using a single boundary measurement [2, 39].

In this framework, the conductivity is assumed to be piecewise constant or piecewise smooth, and it is then convenient to reformulate the problem as a shape optimization problem [61] in order to investigate the sensitivity with respect to perturbations of a trial interface. This sensitivity analysis relies on the calculation of the *shape derivative*, which can be written either in a strong form, usually as a boundary integral, or in a weak form which often presents itself as a domain integral involving the derivative of the perturbation field. The usefulness of the weak form of the shape derivative, often called *domain expression* or *distributed shape derivative*, is known since the pioneering works [20, 37] but has been seldom used since then in comparison with the boundary expression. A revival of the distributed shape derivative has been observed since [10], and this approach has been further developed in the context of EIT and level set methods in [54], see also [29].

An important contribution of the present paper is to extend the framework developed in [54] to the case of point measurements in EIT. The main issue for shape functionals involving point evaluations is that one needs the continuity of the state, for which the usual H^1-regularity in two dimensions is insufficient. Functionals with point evaluations and pointwise constraints have been studied intensively in the optimal control literature; see [32, 66]. In particular, a convenient idea from optimal control is to use Gröger's W^1_p-estimates [30, 31] with $p > 2$ to obtain continuity of the state in two dimensions. Here, we adapt this idea in the context of shape optimization and of the averaged adjoint method, in the spirit of [65]. We show that in general the shape derivative contains Dirac measures, and that the adjoint state is slightly less regular than H^1 due to the presence of Dirac measures on the right-hand side. Another important contribution of this paper is to investigate the relations between the domain and boundary expressions of the shape derivative depending on the interface regularity, and the minimal regularity of the interface for which boundary expressions of the shape derivative can be obtained in the context of EIT with point measurements.

We start by formally describing in section 2 the partial differential equation (PDE) and the inverse problem with point measurements studied in this paper. We consider a conductivity equation with mixed boundary conditions, with a Neumann condition representing an applied current on a part of the boundary and an homogeneous Dirichlet condition on the complementary part. The Dirichlet condition can be used in geophysics to approximate dissipating potentials on regions which are sufficiently far from the source [58, 60], or to model a grounded region such as a grounded electrode in EIT. In section 3, we recall Gröger's W^1_q-estimates for mixed boundary value problems [30], which we use for proving existence of solutions in W^1_q. We then formulate in section 4 the shape optimization approach for the inverse problem of EIT and show how the averaged adjoint method for proving shape differentiability can be adapted to the context of Banach spaces. Then, we compute the distributed shape derivative and prove its validity for conductivity inclusions which are only open. When the inclusion is Lipschitz polygonal or $\mathcal{C}^1$, we also obtain boundary expressions of the shape derivative. Finally, in section 5 we explain the numerical algorithm based on the distributed shape derivative and we present a set of results showing the efficiency of the approach. Introducing an error measure for the reconstruction, we also discuss the quality of reconstructions depending on the number of point measurements, applied boundary currents and noise level. More details about the averaged adjoint method are given in an appendix for the sake of completeness.

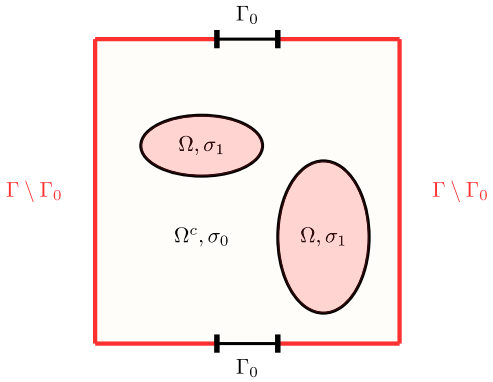

Figure 1. Partition $\mathcal{D} = \Omega \cup \Omega^c$.

2. EIT with point measurements: problem formulation

We start with a formal description of the inverse problem with point measurements considered in this paper. The detailed function space setting will be described afterwards. For sufficiently smooth data, we consider the following conductivity equation with mixed boundary conditions:

$$\begin{aligned} -\mathrm{div}(\sigma \nabla u) &= f \ \text{ in } \mathcal{D}, \\ \partial_n u &= g \ \text{ on } \Gamma, \\ u &= 0 \ \text{ on } \Gamma_0, \end{aligned} \tag{1}$$

where $\mathcal{D} \subset \mathbb{R}^2$ is bounded, $\Gamma \subset \partial\mathcal{D}$ and $\Gamma_0 = \partial\mathcal{D} \setminus \Gamma$.

The boundary value problem (1) is slightly more general than the usual forward model for EIT. In the particular case of EIT, g represents an input, in this case an electric current applied on the boundary of $\mathcal{D}$, u is the corresponding potential, and $f \equiv 0$. Depending on the application, Γ_0 may be interpreted as a grounded region, i.e. $u = 0$ on Γ_0, or as a region distant from the source where the potential u has dissipated to zero. Then, measurements h of the potential on a subset Γ_h of $\overline{\mathcal{D}}$ are performed. In EIT the measurements are usually made on the boundary, i.e. $\Gamma_h \subset \partial\mathcal{D}$, but our results apply to the more general case $\Gamma_h \subset \overline{\mathcal{D}}$. Given the Cauchy data (g, h), the task in EIT is to find the best possible approximation of the unknown conductivity σ. To obtain a better reconstruction, we apply several input currents g_i, $i = 1, \ldots, I$, and the corresponding measurements are denoted by h_i. Denoting u_i the solution of (1) with $g = g_i$, the EIT problem becomes

$$\text{given } \{(g_i, h_i)\}_{i=1}^I, \text{ find } \sigma \text{ such that } u_i = h_i \text{ on } \Gamma_h \quad \text{for } i = 1, \ldots, I. \tag{2}$$

In this paper we study the case of piecewise constant conductivities σ. Let $\Omega \subset \mathcal{D}$ and denote by χ_Ω the characteristic function of Ω, $\Omega^c := \mathcal{D} \setminus \Omega$, and n the outward unit normal vector to Ω. Introduce the piecewise constant conductivity $\sigma_\Omega = \sigma_1 \chi_\Omega + \sigma_0 \chi_{\Omega^c}$, where (σ_0, σ_1) are known positive scalars with $\sigma_1 > \sigma_0$. Note that Ω may have several connected components, as illustrated in figure 1, and we have assumed that $\sigma = \sigma_1$ on each of these components. Observe also that, in this setting, u depends on Ω through σ_Ω. Then, we may recast the EIT problem as the following *shape optimization problem*, in the sense that the geometry Ω is the unknown:

$$\text{given } \{(g_i, h_i)\}_{i=1}^I, \text{ find } \Omega \text{ such that } u_i = h_i \text{ on } \Gamma_h \quad \text{for } i = 1, \ldots, I. \tag{3}$$

The inverse problem (3) is idealized since in practice the measurements h_i are corrupted by noise, therefore we cannot expect that $u_i = h_i$ be exactly achievable, but rather that $|u_i - h_i|$ should be minimized. When Γ_h is a manifold of one or two dimensions, a common approach is to minimize an appropriate cost functional such as

$$J(\Omega) = \frac{1}{2}\sum_{i=1}^{I}\int_{\Gamma_h}(u_i - h_i)^2. \tag{4}$$

Another popular approach is to use a Kohn–Vogelius type functional; see [54].

In this paper we are interested in the case where $\Gamma_h = \{x_k\}_{k=1}^K \subset \overline{\mathcal{D}}$ is a finite set of points, i.e. we only have a finite collection of point measurements. We observe that a Kohn–Vogelius type functional does not seem appropriate for point measurements as this requires to know h on all of $\partial\mathcal{D}$. The functional (4) on the other hand can be adapted to the case $\Gamma_h = \{x_k\}_{k=1}^K$ in the following way. For $i = 1, \ldots, I$, assume that measurements $\{h_i(x_k)\}_{k=1}^K \in \mathbb{R}^K$ are available. For $\Omega \subset \mathcal{D}$ we consider the shape functional

$$J(\Omega) := \frac{1}{2}\sum_{i=1}^{I}\mu_i\sum_{k=1}^{K}\delta_{x_k}((u_i - h_i)^2) = \frac{1}{2}\sum_{i=1}^{I}\mu_i\sum_{k=1}^{K}(u_i(x_k) - h_i(x_k))^2, \tag{5}$$

where $\delta_{x_k} : \mathcal{C}(\overline{\mathcal{D}}) \to \mathbb{R}$ is the Dirac measure concentrated at x_k and μ_i are given constants. The weights μ_i can be used to balance the terms in the sum over the currents indices i. In particular, in our optimization algorithm we choose μ_i as the inverse of $\sum_{k=1}^K (u_i(x_k) - h_i(x_k))^2$ computed at the initial guess. In this way, each term in the sum over $i = 1, \ldots, I$, is equal to 1 at the first iteration, and the initial value of $J(\Omega)$ is equal to $I/2$.

Note that in order to have well-defined point evaluations in the cost function (5), u_i needs to have a higher regularity than the usual H^1-regularity. The main idea of this paper is to work with solutions $u_i \in W_q^1(\mathcal{D})$ with $q > 2$. Indeed, thanks to the continuous embedding $W_q^1(\mathcal{D}) \subset \mathcal{C}(\overline{\mathcal{D}})$ for $q > 2$ in two dimensions, the point evaluation $u_i(x_k)$ in (5) is well-defined.

Without loss of generality, we will compute the shape derivative of $J(\Omega)$ for the simpler case $I = 1$ and $\mu_1 = 1$, in which case the cost functional becomes

$$J(\Omega) = \frac{1}{2}\sum_{k=1}^{K}\delta_{x_k}((u - h)^2) = \frac{1}{2}\sum_{k=1}^{K}(u(x_k) - h(x_k))^2. \tag{6}$$

The formula of the shape derivative in the general case (5) can then be obtained by summation.

3. Mixed boundary value problems in W_q^1

In order to study existence of solutions of (1) in $W_q^1(\mathcal{D})$ for $q > 2$, which allows us to consider point evaluations, we need an appropriate function space setting. We start with several definitions and notations.

Definition 3.1 ([30, 32]). Let $\mathcal{D} \subset \mathbb{R}^2$ and $\Gamma \subset \partial\mathcal{D}$ be given. We say that $\mathcal{D} \cup \Gamma$ is regular (in the sense of Gröger) if $\mathcal{D}$ is a bounded Lipschitz domain, Γ is a relatively open part of the boundary $\partial\mathcal{D}$, $\Gamma_0 := \partial\mathcal{D}\backslash\Gamma$ has positive measure, and Γ_0 is a finite union of closed and nondegenerate (i.e., not a single point) curved pieces of $\partial\mathcal{D}$. The set of regular domains in the sense of Gröger is denoted

$$\Xi := \{(\mathcal{D}, \Gamma) \mid \mathcal{D} \subset \mathbb{R}^2, \Gamma \subset \partial\mathcal{D}, \text{ and } \mathcal{D} \cup \Gamma \text{ is regular}\}. \tag{7}$$

We also define

$$\mathbb{P}(\mathcal{D}) := \{\Omega \subset \mathcal{D} \mid \Omega \text{ open and compactly contained in } \mathcal{D}\}. \tag{8}$$

Definition 3.2 ($W_q^1(\mathcal{D})$ **spaces).** Let $(\mathcal{D},\Gamma) \in \Xi$ and $\Gamma_0 := \partial\mathcal{D}\backslash\Gamma$. For $d \geqslant 1$ we define

$$\mathcal{C}_\Gamma^\infty(\mathcal{D},\mathbb{R}^d) := \{f|_\mathcal{D} \mid f \in \mathcal{C}^\infty(\mathbb{R}^2,\mathbb{R}^d),\ \text{supp} f \cap \Gamma_0 = \emptyset\}.$$

In the scalar case, i.e. for $d = 1$, we write $\mathcal{C}_\Gamma^\infty(\mathcal{D})$ instead of $\mathcal{C}_\Gamma^\infty(\mathcal{D},\mathbb{R})$ and use a similar notation for the other function spaces. We denote by $W_q^1(\mathcal{D})$, $1 \leqslant q \leqslant \infty$ the Sobolev space of weakly differentiable functions with weak derivative in $L^q(\mathcal{D})$. For $q, q' \geqslant 1$ satisfying $\frac{1}{q} + \frac{1}{q'} = 1$, we define the Sobolev space

$$W_{\Gamma,q}^1(\mathcal{D},\mathbb{R}^d) := \overline{\mathcal{C}_\Gamma^\infty(\mathcal{D},\mathbb{R}^d)}^{W_q^1},$$

where W_q^1 stands for the usual norm in $W^{1,q}(\mathcal{D},\mathbb{R}^d)$, and the dual space

$$W_{\Gamma,q}^{-1}(\mathcal{D},\mathbb{R}^d) := (W_{\Gamma,q'}^1(\mathcal{D},\mathbb{R}^d))^*.$$

Notations. The notation id denotes the identity function in $\mathbb{R}^2$, and $\mathbb{I}$ is the 2×2 identity matrix.

We can now state the variational formulation corresponding to the strong formulation of the mixed boundary value problem (1) in the appropriate function space: find $u \in W_{\Gamma,q}^1(\mathcal{D})$ solution of

$$\int_\mathcal{D} \sigma\nabla u \cdot \nabla v = \int_\mathcal{D} fv + \int_\Gamma gv \quad \text{for all} \quad v \in W_{\Gamma,q'}^1(\mathcal{D}), \tag{9}$$

with $(\mathcal{D},\Gamma) \in \Xi$, $g \in L^\infty(\partial\mathcal{D})$, $f \in L^q(\mathcal{D})$ and the conductivity $\sigma \in L^\infty(\mathcal{D})$ satisfying $\sigma \geqslant \underline{\sigma} > 0$.

In order to study existence of solutions for (9), we recall the framework introduced in [30] for obtaining a W_q^1-estimate for solutions to mixed boundary value problems for second order elliptic PDEs. Let $2 \leqslant q < \infty$ and $1 \leqslant q' \leqslant 2$ satisfying $\frac{1}{q} + \frac{1}{q'} = 1$. Let $\mathbb{A} \in L^\infty(\mathcal{D},\mathbb{R}^{2\times 2})$ be a matrix-valued function satisfying for all $\eta, \theta \in \mathbb{R}^2$ and $x \in \overline{\mathcal{D}}$:

$$\mathbb{A}(x)\theta \cdot \theta \geqslant m|\theta|^2 \quad \text{and} \quad |\mathbb{A}(x)\eta| \leqslant M|\eta|, \quad \text{with} \quad m > 0 \quad \text{and} \quad M > 0, \tag{10}$$

where $|\cdot|$ denotes the Euclidean norm and $m \leqslant M$. Introduce

$$\begin{aligned} a : W_{\Gamma,q}^1(\mathcal{D}) \times W_{\Gamma,q'}^1(\mathcal{D}) &\to \mathbb{R} \\ (v,w) &\mapsto \int_\mathcal{D} \mathbb{A}\nabla v \cdot \nabla w. \end{aligned} \tag{11}$$

Then, define the corresponding operator

$$\begin{aligned} \mathcal{A}_q : W_{\Gamma,q}^1(\mathcal{D}) &\to W_{\Gamma,q}^{-1}(\mathcal{D}), \\ v &\mapsto \mathcal{A}_q v := a(v,\cdot). \end{aligned} \tag{12}$$

Let $\mathcal{P}$ be defined by, for $u, v \in W_{\Gamma,2}^1(\mathcal{D})$,

$$\langle \mathcal{P}u, v\rangle := \int_\mathcal{D} \nabla u \cdot \nabla v + uv.$$

By Hölder's inequality it follows that $\mathcal{P} : W^1_{\Gamma,q}(\mathcal{D}) \to W^{-1}_{\Gamma,q}(\mathcal{D})$ is a well-defined and continuous operator for all $q \geqslant 2$. We also introduce the constant

$$M_q := \sup\{\|v\|_{W^1_q(\mathcal{D})} \mid v \in W^1_{\Gamma,q}(\mathcal{D}), \|\mathcal{P}v\|_{W^{-1}_{\Gamma,q}(\mathcal{D})} \leqslant 1\}.$$

It is easily verified that $M_2 = 1$.

Definition 3.3. Denote by R_q, $2 \leqslant q < \infty$, the set of regular domains $(\mathcal{D}, \Gamma) \in \Xi$ for which $\mathcal{P}$ maps $W^1_{\Gamma,q}(\mathcal{D})$ onto $W^{-1}_{\Gamma,q}(\mathcal{D})$.

We can now state an adapted version of [31, theorem 1] which plays a key role in our investigations. The principal application of theorem 3.4 is to prove existence of solutions u in the space $W^1_{\Gamma,q}(\mathcal{D})$ for the conductivity equation (9), with $q > 2$. Recall that thanks to the continuous embedding $W^1_{\Gamma,q}(\mathcal{D}) \subset \mathcal{C}(\overline{\mathcal{D}})$, the $W^1_{\Gamma,q}$-regularity of u allows us to work with the point evaluations $u(x_k)$, where $\{x_k\}_{k=1}^K$ are the positions of the point measurements.

Theorem 3.4 [31, theorem 1]. *Let $(\mathcal{D}, \Gamma) \in R_{q_0}$ for some $q_0 > 2$. Suppose that $\mathbb{A}$ satisfies conditions (10) for q_0 and let $\mathcal{A}_q$ be defined by (12). Then $\mathcal{A}_q : W^1_{\Gamma,q}(\mathcal{D}) \to W^{-1}_{\Gamma,q}(\mathcal{D})$ is an isomorphism provided that $q \in [2, q_0]$ and $M_q k < 1$, where $k := (1 - m^2/M^2)^{1/2}$, and*

$$\|\mathcal{A}_q^{-1}\|_{L(W^{-1}_{\Gamma,q}(\mathcal{D}), W^1_{\Gamma,q}(\mathcal{D}))} \leqslant c_q, \tag{13}$$

where $c_q := mM^{-2}M_q(1 - M_q k)^{-1}$. Finally, $M_q k < 1$ is satisfied if

$$\frac{1}{q} > \frac{1}{2} - \left(\frac{1}{2} - \frac{1}{q_0}\right)\frac{|\log\ k|}{\log\ M_{q_0}}.$$

Remark 3.5.

- If $(\mathcal{D}, \Gamma) \in R_q$, then $M_q < \infty$.
- For every regular $(\mathcal{D}, \Gamma) \in \Xi$, there exists a $q_0 > 2$ so that $(\mathcal{D}, \Gamma) \in R_{q_0}$; see [30, theorem 3].
- For sufficiently small $q > 2$, the constant c_q in (13) can be chosen to be independent of q; see [65, corollary 5].

We now explain how a particular case of the theory described in this section can be applied to the EIT problem with point measurements. Let $(\mathcal{D}, \Gamma) \in \Xi$ and suppose that the conductivity $\sigma \in L^\infty(\mathcal{D})$ satisfies pointwise a.e. $\overline{\sigma} \geqslant \sigma \geqslant \underline{\sigma} > 0$, where $\overline{\sigma}, \underline{\sigma} > 0$ are constants. It is clear that $\mathbb{A} := \sigma\mathbb{I} \in L^\infty(\mathcal{D}, \mathbb{R}^{2\times 2})$ satisfies conditions (10). In view of remark 3.5, there exists $q_0 > 2$ such that $(\mathcal{D}, \Gamma) \in R_{q_0}$. For $q \in [2, q_0]$, $f \in L^q(\mathcal{D})$ and $g \in L^\infty(\partial\mathcal{D})$, the functional

$$\langle F, v\rangle := \int_{\mathcal{D}} fv + \int_\Gamma gv, \quad v \in W^1_{\Gamma,q'}(\mathcal{D}),$$

defines an element in $(W^1_{\Gamma,q'}(\mathcal{D}))^* = W^{-1}_{\Gamma,q}(\mathcal{D})$.

In view of (11), (12) and $\mathbb{A} := \sigma\mathbb{I}$, we have

$$\langle \mathcal{A}_q u, v\rangle_{W^{-1}_{\Gamma,q}(\mathcal{D}), W^1_{\Gamma,q'}(\mathcal{D})} = \int_{\mathcal{D}} \sigma\nabla u \cdot \nabla v.$$

Thus, the equation: find $u \in W^1_{\Gamma,q}(\mathcal{D})$ such that

$$\int_{\mathcal{D}} \sigma\nabla u \cdot \nabla v = \int_{\mathcal{D}} fv + \int_\Gamma gv \quad \text{for all } v \in W^1_{\Gamma,q'}(\mathcal{D}),$$

can be written as $\langle \mathcal{A}_q u, v\rangle_{W^{-1}_{\Gamma,q}(\mathcal{D}),W^{1}_{\Gamma,q'}(\mathcal{D})} = \langle F, v\rangle_{W^{-1}_{\Gamma,q}(\mathcal{D}),W^{1}_{\Gamma,q'}(\mathcal{D})}$. Since $\mathcal{A}_q : W^1_{\Gamma,q}(\mathcal{D}) \to W^{-1}_{\Gamma,q}(\mathcal{D})$ is an isomorphism if the conditions of theorem 3.4 are satisfied, there is a unique $u \in W^1_{\Gamma,q}(\mathcal{D})$ solution to

$$\int_{\mathcal{D}} \sigma \nabla u \cdot \nabla v = \int_{\mathcal{D}} fv + \int_{\Gamma} gv \quad \text{for all } v \in W^1_{\Gamma,q'}(\mathcal{D}),$$

provided $q \in]2, q_0]$ is sufficiently close to 2.

4. Shape optimization

In this section we start by recalling the definition of the Eulerian shape derivative, then we apply the averaged adjoint method to prove the shape differentiability of the cost functional $J(\Omega)$ and compute the shape derivative.

Let $(\mathcal{D}, \Gamma) \in \Xi$, for $k \geqslant 0$ we define

$$\mathcal{C}^k_c(\mathcal{D}, \mathbb{R}^2) := \{V \in \mathcal{C}^k(\mathcal{D}, \mathbb{R}^2) \mid V \text{ has compact support in } \mathcal{D}\},$$

and $\mathcal{C}^\infty_c(\mathcal{D}, \mathbb{R}^2)$ similarly, and we equip these spaces with their usual topologies; see [1, 1.56, pp 19–20]. Consider a vector field $V \in \mathcal{C}^1_c(\mathcal{D}, \mathbb{R}^2)$ and the associated flow $T_t : \mathcal{D} \to \mathcal{D}$, $t \in [0, t_0]$ for some $t_0 > 0$, defined for each $x_0 \in \mathcal{D}$ as $T_t(x_0) := x(t)$, where $x : [0, t_0] \to \mathbb{R}^d$ solves

$$\dot{x}(t) = V(x(t)) \quad \text{for} \quad t \in [0, t_0],\ x(0) = x_0. \tag{14}$$

For $\Omega \in \mathbb{P}(\mathcal{D})$, we consider the family of perturbed domains

$$\Omega_t := T_t(\Omega). \tag{15}$$

Definition 4.1 (Shape derivative). Let $J : \mathbb{P}(\mathcal{D}) \to \mathbb{R}$ be a shape functional.

(a) The Eulerian semiderivative of J at Ω in direction $V \in \mathcal{C}^1_c(\mathcal{D}, \mathbb{R}^2)$ is defined by, when the limit exists,

$$dJ(\Omega)(V) := \lim_{t \searrow 0} \frac{J(\Omega_t) - J(\Omega)}{t}. \tag{16}$$

(b) J is *shape differentiable* at Ω if it has a Eulerian semiderivative at Ω for all $V \in \mathcal{C}^\infty_c(\mathcal{D}, \mathbb{R}^2)$ and the mapping

$$dJ(\Omega) : \mathcal{C}^\infty_c(\mathcal{D}, \mathbb{R}^2) \to \mathbb{R},\ V \mapsto dJ(\Omega)(V)$$

is linear and continuous, in which case $dJ(\Omega)(V)$ is called the *Eulerian shape derivative* at Ω, or simply *shape derivative* at Ω.

4.1. Distributed shape derivative via averaged adjoint method

The averaged adjoint method is a Lagrangian-type approach introduced in [64] to compute the derivative of shape functionals with PDE constraints. In this section we apply this method to compute the distributed shape derivative of $J(\Omega)$. We refer to the appendix for a detailed description of the method.

For $\Omega \in \mathbb{P}(\mathcal{D})$ (see (8)) and $V \in \mathcal{C}^1_c(\mathcal{D}, \mathbb{R}^2)$, define Ω_t as in (15). Since V has compact support in $\mathcal{D}$, we have $\Omega_t \subset \mathcal{D}$ for all $t \in [0, t_0]$. In the rest of the paper, we assume that the conductivity is piecewise constant, i.e. $\sigma_\Omega = \sigma_1 \chi_\Omega + \sigma_0 \chi_{\Omega^c}$, where (σ_0, σ_1) are positive scalars with $\sigma_1 > \sigma_0$, and also that $f_\Omega = f_1 \chi_\Omega + f_0 \chi_{\Omega^c}$ where $f_0, f_1 \in H^1(\mathcal{D})$.

We consider the Lagrangian $\mathcal{L} : \mathbb{P}(\mathcal{D}) \times W^1_{\Gamma,q}(\mathcal{D}) \times W^1_{\Gamma,q'}(\mathcal{D}) \to \mathbb{R}$ associated with the cost functional (6) and the PDE constraint in variational form (9) defined by

$$\mathcal{L}(\Omega, \varphi, \psi) := \frac{1}{2}\sum_{k=1}^{K} (\varphi(x_k) - h(x_k))^2 + \int_{\mathcal{D}} \sigma_\Omega \nabla\varphi \cdot \nabla\psi - f_\Omega \psi - \int_\Gamma g\psi. \quad (17)$$

Following the methodology of the averaged adjoint method (see appendix for details), we introduce the *shape-Lagrangian* $G : [0, t_0] \times W^1_{\Gamma,q}(\mathcal{D}) \times W^1_{\Gamma,q'}(\mathcal{D}) \to \mathbb{R}$ as

$$\begin{aligned} G(t, \varphi, \psi) &:= \mathcal{L}(\Omega_t, \varphi \circ T_t^{-1}, \psi \circ T_t^{-1}) \\ &= \frac{1}{2}\sum_{k=1}^{K} (\varphi \circ T_t^{-1} - h)^2(x_k) + \int_{\mathcal{D}} \sigma_{\Omega_t} \nabla(\varphi \circ T_t^{-1}) \cdot \nabla(\psi \circ T_t^{-1}) - f_{\Omega_t} \psi \circ T_t^{-1} \\ &\quad - \int_\Gamma g\psi \circ T_t^{-1}. \end{aligned}$$

Notice that for all $q \geqslant 1$ we have $\varphi \in W^1_{\Gamma,q}(\mathcal{D})$ if and only if $\varphi \circ T_t \in W^1_{\Gamma,q}(\mathcal{D})$; see [68, theorem 2.2.2, p 52]. Observe that

$$\sigma_{\Omega_t} \circ T_t = \sigma_1 \chi_{\Omega_t} \circ T_t + \sigma_0 \chi_{\Omega_t^c} \circ T_t = \sigma_1 \chi_\Omega + \sigma_0 \chi_{\Omega^c} = \sigma_\Omega.$$

We also introduce the notation

$$f^t := f_{\Omega_t} \circ T_t = f_1 \circ T_t \, \chi_{\Omega_t} \circ T_t + f_0 \circ T_t \, \chi_{\Omega_t^c} \circ T_t = f_1 \circ T_t \, \chi_\Omega + f_0 \circ T_t \, \chi_{\Omega^c}. \quad (18)$$

Using the fact that $T_t = \mathrm{id}$ on $\partial\mathcal{D}$ and proceeding with the change of variables $x \mapsto T_t(x)$ inside the integrals in $G(t, \varphi, \psi)$, we obtain using the chain rule

$$G(t, \varphi, \psi) = \frac{1}{2}\sum_{k=1}^{K} (\varphi \circ T_t^{-1} - h)^2(x_k) + \int_{\mathcal{D}} \sigma_\Omega A(t) \nabla\varphi \cdot \nabla\psi - f^t \psi - \int_\Gamma g\psi, \quad (19)$$

where

$$A(t) := \det(DT_t) DT_t^{-1} DT_t^{-\mathsf{T}}. \quad (20)$$

For $t \in [0, t_0]$, let us define the perturbation $\mathcal{A}^t_q$ of $\mathcal{A}_q$ defined in (12) as follows:

$$\begin{aligned} &\mathcal{A}^t_q : W^1_{\Gamma,q}(\mathcal{D}) \to W^{-1}_{\Gamma,q}(\mathcal{D}), \\ &\qquad v \mapsto \left(w \mapsto \langle \mathcal{A}^t_q v, w \rangle := \int_{\mathcal{D}} \sigma_\Omega A(t) \nabla v \cdot \nabla w \right). \end{aligned} \quad (21)$$

By continuity of $t \mapsto A(t) : [0, t_0] \to \mathcal{C}(\overline{\mathcal{D}}, \mathbb{R}^{2\times 2})$, for every $\epsilon > 0$ there exists $\delta > 0$ so that the following result (see [65, lemma 13]) follows immediately:

$$A(t)(x)\eta \cdot \eta \geqslant (1 - \epsilon)|\eta|^2 \quad \text{for all} \quad \eta \in \mathbb{R}^2 \quad \text{and all} \quad (t, x) \in [0, \delta] \times \overline{\mathcal{D}}, \quad (22)$$

$$|A(t)(x)| \leqslant 1 + \epsilon \quad \text{for all} \quad (t, x) \in [0, \delta] \times \overline{\mathcal{D}}. \quad (23)$$

The core element of the averaged adjoint method is the so-called *averaged adjoint* p^t defined in (55), which is the solution to a PDE involving the adjoint of the operator $\mathcal{A}_q^t$; see the proof of theorem 4.3 for more details. In order to obtain a solution of the averaged adjoint equation in the desired space $W^1_{\Gamma,q}(\mathcal{D})$, we need the following perturbed version of theorem 3.4, showing that $\mathcal{A}_q^t$ is an isomorphism for t in a small neighbourhood of 0. We also need this result to prove existence of a solution for the perturbed state $u^t \in W^1_{\Gamma,q}(\mathcal{D})$, see (31). Such a result can be achieved using properties (22) and (23).

Theorem 4.2. *For each $(\mathcal{D},\Gamma) \in \Xi$ there exists $q_0 > 2$, $\epsilon > 0$ and $\delta > 0$ so that for all $t \in [0,\delta]$ and all $q \in [2,q_0]$ satisfying $M_q k < 1$, where $k := (1 - m^2/M^2)^{1/2} < 1$ with $m = \sigma_0(1-\epsilon)$ and $M = \sigma_1(1+\epsilon)$, the mapping $\mathcal{A}_q^t : W^1_{\Gamma,q}(\mathcal{D}) \to W^{-1}_{\Gamma,q}(\mathcal{D})$ defined by (21) is an isomorphism. Moreover, we have for all $t \in [0,\delta]$ that*

$$\|(\mathcal{A}_q^t)^{-1}\|_{L(W^{-1}_{\Gamma,q}(\mathcal{D}),W^1_{\Gamma,q}(\mathcal{D}))} \leqslant c_q, \tag{24}$$

where $c_q := mM^{-2}M_q(1-M_q k)^{-1}$ is independent of t. Finally, $M_q k < 1$ is satisfied if

$$\frac{1}{q} > \frac{1}{2} - \left(\frac{1}{2} - \frac{1}{q_0}\right)\frac{|\log\ k|}{\log\ M_{q_0}}.$$

Proof. We have $\sigma_1 \geqslant \sigma \geqslant \sigma_0 > 0$ with $\sigma_0 < \sigma_1$. Let us choose $\epsilon < 1$ and δ such that (22), (23) is satisfied, and let $t \in [0,\delta)$. In view of (22), (23) it immediately follows that $\mathbb{A} = \sigma_\Omega A(t) \in L^\infty(\mathcal{D},\mathbb{R}^{2\times 2})$ satisfies assumptions (10) with $m = \sigma_0(1-\epsilon)$ and $M = \sigma_1(1+\epsilon)$. Hence, the result follows directly from theorem 3.4, since M and m are independent of t. □

The main statement of this section is the following theorem 4.3, for which we first need several notations.

Notations. For vectors $a \in \mathbb{R}^d$ and $b \in \mathbb{R}^d$, the outer product $a \otimes b$ is defined as the second order tensor with entries $[a \otimes b]_{ij} = a_i b_j$ and the symmetric outer product as $a \odot b := (a \otimes b + b \otimes a)/2$. For second order tensors $\mathbf{S} \in \mathbb{R}^{d\times d}$ and $\mathbf{T} \in \mathbb{R}^{d\times d}$ whose entries are denoted by $\mathbf{S}_{ij}$ and $\mathbf{T}_{ij}$, the double dot product of $\mathbf{S}$ and $\mathbf{T}$ is defined as $\mathbf{S} : \mathbf{T} = \sum_{i,j=1}^d \mathbf{S}_{ij}\mathbf{T}_{ij}$.

Theorem 4.3 (distributed shape derivative). *Let $\mathcal{D} \cup \Gamma \subset \mathbb{R}^2$ be a regular domain in the sense of Gröger, $\Omega \in \mathbb{P}(\mathcal{D})$ (see (8)) and $J : \mathbb{P}(\mathcal{D}) \to \mathbb{R}$ be defined in (6). Assume that $\Gamma_h \cap \partial\Omega = \emptyset$ and $f_\Omega = f_1\chi_\Omega + f_0\chi_{\Omega^c}$ where $f_0, f_1 \in H^1(\mathcal{D})$. Then the shape derivative of J at Ω in direction $V \in \mathcal{C}^1_c(\mathcal{D},\mathbb{R}^2)$ is given by*

$$dJ(\Omega)(V) = \mathbf{S}_0(V) + \int_{\mathcal{D}} \mathbf{S}_1 : DV, \tag{25}$$

where $\mathbf{S}_1 \in L^1(\mathcal{D},\mathbb{R}^{2\times 2})$ and $\mathbf{S}_0 \in (\mathcal{C}(\overline{\mathcal{D}},\mathbb{R}^2))^*$ are defined by

$$\mathbf{S}_1 = -2\sigma_\Omega \nabla u \odot \nabla p + (\sigma_\Omega \nabla u \cdot \nabla p - f_\Omega p)\mathbb{I}, \tag{26}$$

$$\mathbf{S}_0(V) = \mathbf{S}_0^s(V) + \int_{\mathcal{D}} \mathbf{S}_0^r \cdot V, \tag{27}$$

$$\mathbf{S}_0^r = -p\widetilde{\nabla} f_\Omega, \tag{28}$$

$$\mathbf{S}_0^s = -\sum_{k=1}^K ((u-h)\nabla u)(x_k)\delta_{x_k}, \tag{29}$$

where $\widetilde{\nabla} f_\Omega := \nabla f_1\, \chi_\Omega + \nabla f_0\, \chi_{\Omega^c}$ *and* $\mathbf{S}_0^r \in L^1(\mathcal{D}, \mathbb{R}^2)$.

Also, there exists $q > 2$ *such that the adjoint* $p \in W^1_{\Gamma,q'}(\mathcal{D})$ *is the solution to*

$$\int_{\mathcal{D}} \sigma_\Omega \nabla p \cdot \nabla \varphi = -\sum_{k=1}^{K} (u(x_k) - h(x_k))\varphi(x_k) \quad \textit{for all } \varphi \in W^1_{\Gamma,q}(\mathcal{D}). \tag{30}$$

Proof. We employ the averaged adjoint approach of [64] and follow the arguments of [65], we refer to the appendix for details about the method. Let us define the perturbed state $u^t \in W^1_{\Gamma,q}(\mathcal{D})$ solution of

$$\int_{\mathcal{D}} \sigma_\Omega A(t) \nabla u^t \cdot \nabla \varphi = \int_{\mathcal{D}} f^t \varphi + \int_\Gamma g\varphi \quad \text{for all} \quad \varphi \in W^1_{\Gamma,q'}(\mathcal{D}), \tag{31}$$

where f^t is defined in (18) and $A(t)$ in (20). The mapping $F_t : W^1_{\Gamma,q'}(\mathcal{D}) \to \mathbb{R}$ defined by

$$\langle F_t, v\rangle := \int_{\mathcal{D}} f^t v + \int_\Gamma g v \quad \text{for} \quad v \in W^1_{\Gamma,q'}(\mathcal{D})$$

is well-defined and continuous. Consequently, thanks to theorem 4.2 there is a unique solution to (31) in $W^1_{\Gamma,q}(\mathcal{D})$ for $q > 2$ sufficiently close to 2. Using (24) we get

$$\|u^t\|_{W^1_{\Gamma,q}(\mathcal{D})} \leqslant c_q \|F_t\|_{W^{-1}_{\Gamma,q}(\mathcal{D})} \leqslant C(\|f^t\|_{L^2(\mathcal{D})} + \|g\|_{L^\infty(\partial\mathcal{D})}).$$

It follows that for some constant C independent of t, we have

$$\|u^t\|_{W^1_{\Gamma,q}(\mathcal{D})} \leqslant C. \tag{32}$$

Following (55), the *averaged adjoint equation* reads: find $p^t \in W^1_{\Gamma,q'}(\mathcal{D})$, such that

$$\int_0^1 d_\varphi G(t, su^t + (1-s)u^0; p^t)(\varphi)\, \mathrm{d}s = 0 \quad \text{for all} \quad \varphi \in W^1_{\Gamma,q}(\mathcal{D}), \tag{33}$$

which is equivalent to, using the fact that $A(t)^\mathsf{T} = A(t)$,

$$\begin{aligned}\int_{\mathcal{D}} \sigma_\Omega A(t) \nabla p^t \cdot \nabla \varphi \\ = \frac{1}{2}\sum_{k=1}^{K} (u^t \circ T_t^{-1}(x_k) + u^0 \circ T_t^{-1}(x_k) - 2h(x_k))\varphi \circ T_t^{-1}(x_k) \quad \text{for all } \varphi \in W^1_{\Gamma,q}(\mathcal{D}).\end{aligned} \tag{34}$$

In view of the definition (21) of $\mathcal{A}_q^t$, the adjoint operator is defined as

$$\begin{aligned}(\mathcal{A}_q^t)^* : W^{-1}_{\Gamma,q}(\mathcal{D})^* = W^1_{\Gamma,q'}(\mathcal{D}) \to W^1_{\Gamma,q}(\mathcal{D})^* = W^{-1}_{\Gamma,q'}(\mathcal{D}), \\ w \mapsto \left(v \mapsto \langle (\mathcal{A}_q^t)^* w, v\rangle := \langle w, \mathcal{A}_q^t v\rangle\right).\end{aligned} \tag{35}$$

Using (21) and the fact that $A(t)^\mathsf{T} = A(t)$ we get for $w \in W^1_{\Gamma,q'}(\mathcal{D})$ and $v \in W^1_{\Gamma,q}(\mathcal{D})$,

$$\langle (\mathcal{A}_q^t)^* w, v\rangle = \int_{\mathcal{D}} \sigma_\Omega A(t) \nabla w \cdot \nabla v.$$

Now, in view of theorem 4.2 there exists $q > 2$ and $\delta > 0$ such that the mapping $\mathcal{A}_q^t : W^1_{\Gamma,q}(\mathcal{D}) \to W^{-1}_{\Gamma,q}(\mathcal{D})$ is an isomorphism for all $t \in [0, \delta]$. Thus, the adjoint mapping $(\mathcal{A}_q^t)^* : W^1_{\Gamma,q'}(\mathcal{D}) \to W^{-1}_{\Gamma,q'}(\mathcal{D})$ is also an isomorphism.

Now the functional $R_t : W^1_{\Gamma,q}(\mathcal{D}) \to \mathbb{R}$ defined by

$$\langle R_t, v\rangle := \frac{1}{2}\sum_{k=1}^{K}(u^t \circ T_t^{-1}(x_k) + u^0 \circ T_t^{-1}(x_k) - 2h(x_k))v \circ T_t^{-1}(x_k) \quad \text{for} \quad v \in W^1_{\Gamma,q}(\mathcal{D}).$$

is well-defined and continuous. Therefore, since $(\mathcal{A}_q^t)^*$ is an isomorphism, the averaged adjoint equation (34), which can be written as $(\mathcal{A}_q^t)^* p^t = R_t$, has a unique solution $p^t \in W^1_{\Gamma,q'}(\mathcal{D})$.

Using the continuous embedding of $W^1_{\Gamma,q}(\mathcal{D})$ into the space of continuous functions $\mathcal{C}(\overline{\mathcal{D}})$ for $q > 2$ in two dimensions, it also follows that

$$\begin{aligned}\|p^t\|_{W^1_{\Gamma,q'}(\mathcal{D})} &\leqslant C \max_{k\in\{1,\dots,K\}} |(u^t \circ T_t^{-1} + u^0 \circ T_t^{-1} - 2h)(x_k)| \\ &\leqslant C\left(\|u^t\|_{W^1_{\Gamma,q}(\mathcal{D})} + \|u^0\|_{W^1_{\Gamma,q}(\mathcal{D})} + \max_{k\in\{1,\dots,K\}} |h(x_k)|\right).\end{aligned}$$

Then using (32) we get, for some constant C independent of t,

$$\|p^t\|_{W^1_{\Gamma,q'}(\mathcal{D})} \leqslant C. \tag{36}$$

The estimate (36) yields that $p^t \rightharpoonup p^0$ weakly in $W^1_{\Gamma,q'}(\mathcal{D})$ as $t \searrow 0$. Using (56) and the fact that $G(0, u^0, p^0) = G(0, u^0, \psi)$ for all $\psi \in W^1_{\Gamma,q'}(\mathcal{D})$, we have

$$\frac{G(t, u^t, p^t) - G(0, u^0, p^0)}{t} = \frac{G(t, u^0, p^t) - G(0, u^0, p^t)}{t}, \tag{37}$$

and then, in view of (19),

$$\begin{aligned}\frac{G(t, u^0, p^t) - G(0, u^0, p^t)}{t} &= \frac{1}{2}\sum_{k=1}^{K}\frac{(u^0 \circ T_t^{-1} - h)^2(x_k) - (u^0 - h)^2(x_k)}{t} \\ &\quad + \int_{\mathcal{D}} \sigma_\Omega \frac{A(t) - \mathbb{I}}{t}\nabla u^0 \cdot \nabla p^t - \frac{f^t - f^0}{t}p^t.\end{aligned} \tag{38}$$

Using the assumption $\Gamma_h \cap \partial\Omega = \emptyset$, we have for all $k = 1, \dots, K$ that x_k belongs either to Ω, to $\mathcal{D}\backslash\overline{\Omega}$ or to $\partial\mathcal{D}$. Assume first that x_k belongs either to Ω or to $\mathcal{D}\backslash\overline{\Omega}$. Since σ_Ω is constant in Ω and in $\mathcal{D}\backslash\overline{\Omega}$, u is harmonic in these sets, therefore using elliptic regularity results we have $u \in \mathcal{C}^\infty(B(x_k, r_k))$ for sufficiently small r_k, where $B(x_k, r_k)$ denotes the open ball of centre x_k and radius r_k. Thus, the first term on the right-hand side of (38) converges as $t \searrow 0$. Now if $x_k \in \partial\mathcal{D}$, then $T_t(x_k) = x_k$ due to $V \in \mathcal{C}^1_c(\mathcal{D}, \mathbb{R}^2)$, and the first term on the right-hand side of (38) is equal to zero, so we obtain the same formula as in the case $x_k \in \mathcal{D}\backslash\overline{\Omega}$. Also, using $V \in \mathcal{C}^1_c(\mathcal{D}, \mathbb{R}^2)$ we have the following convergence properties (see [47, lemma 3.1] and [63, lemma 2.16])

$$\frac{A(t) - \mathbb{I}}{t} \to A'(0) := \operatorname{div}(V) - DV - DV^{\mathsf{T}} \quad \text{strongly in} \quad \mathcal{C}(\overline{\mathcal{D}}, \mathbb{R}^{2\times 2}), \tag{39}$$

$$\frac{f^t - f^0}{t} \to f_\Omega \operatorname{div}(V) + \widetilde{\nabla} f_\Omega \cdot V \quad \text{strongly in} \quad L^2(\mathcal{D}), \tag{40}$$

and we conclude that the right-hand side of (38) converges to

$$-\sum_{k=1}^{K}(u^0-h)(x_k)\nabla u^0(x_k)\cdot V(x_k)+\int_{\mathcal{D}}\sigma_\Omega A'(0)\nabla u^0\cdot\nabla p^0-(f_\Omega\,\mathrm{div}(V)+\widetilde{\nabla}f_\Omega\cdot V)p^0. \quad (41)$$

In view of (19), (37) and (38) this shows

$$\lim_{t\searrow 0}\frac{G(t,u^t,p^t)-G(0,u^0,p^0)}{t}=\partial_t G(0,u^0,p^0), \quad (42)$$

which shows that assumption 6.2 is satisfied.

Using tensor calculus, the property $\mathrm{div}(V)=\mathbb{I}:DV$, the notations $u=u^0$ and $p=p^0$, we can further transform (41) in the following way:

$$\begin{aligned}\sigma_\Omega A'(0)\nabla u\cdot\nabla p&=\sigma_\Omega\,\mathrm{div}(V)\nabla u\cdot\nabla p-\sigma_\Omega DV\nabla u\cdot\nabla p-\sigma_\Omega DV^{\mathsf{T}}\nabla u\cdot\nabla p\\&=\sigma_\Omega(\nabla u\cdot\nabla p)\mathbb{I}:DV-\sigma_\Omega DV:(\nabla p\otimes\nabla u)-\sigma_\Omega DV:(\nabla u\otimes\nabla p)\\&=\sigma_\Omega((\nabla u\cdot\nabla p)\mathbb{I}-2\nabla u\odot\nabla p):DV,\end{aligned}$$

and $(f_\Omega\,\mathrm{div}(V)+\widetilde{\nabla}f_\Omega\cdot V)p^0=(f_\Omega p\mathbb{I}):DV+p\widetilde{\nabla}f_\Omega\cdot V$. Gathering these results, (41) can be brought into expression (25).

The regularity $\mathbf{S}_1\in L^1(\mathcal{D},\mathbb{R}^{2\times 2})$ is due to $u\in W^1_{\Gamma,q}(\mathcal{D})$, $p\in W^1_{\Gamma,q'}(\mathcal{D})$ and $f_\Omega\in L^q(\mathcal{D})$, and the regularity of $\mathbf{S}_0^r$ is a consequence of the regularity of p and f_Ω. □

4.2. Boundary expression of the shape derivative

An interesting feature of theorem 4.3 is to show that the distributed shape derivative exists even when Ω is only open. Another relevant issue is to determine the minimal regularity of Ω for which boundary expressions of the shape derivative can be obtained. This section is devoted to the study of this question. We start with the following well-known result which describes the structure of the boundary expression of the shape derivative; see [21, pp 480–481].

Theorem 4.4 (Zolésio's structure theorem). *Let Ω be open with $\partial\Omega$ compact and of class $\mathcal{C}^{k+1}$, $k\geqslant 0$. Assume J has a Eulerian shape derivative at Ω and $dJ(\Omega)$ is continuous for the $\mathcal{C}^k(\mathcal{D},\mathbb{R}^d)$-topology. Then, there exists a linear and continuous functional $l:\mathcal{C}^k(\partial\Omega)\to\mathbb{R}$ such that*

$$dJ(\Omega)(V)=l(V_{|\partial\Omega}\cdot n)\quad \textit{for all}\quad V\in\mathcal{C}^k_c(\mathcal{D},\mathbb{R}^d). \quad (43)$$

Theorem 4.4 requires Ω to be at least $\mathcal{C}^1$, however we show in proposition 4.5 that even for Lipschitz domains one can obtain a boundary expression for the shape derivative, see (47), even though we get a weaker structure than (43) since the tangential component of V may be present in (47). Recall that a bounded domain is called Lipschitz if it is locally representable as the graph of a Lipschitz function. In this case, it is well-known that the surface measure is well-defined on $\partial\Omega$ and there exists an outward pointing normal vector n at almost every point on $\partial\Omega$; see [23, section 4.2, p 127].

Notations. For $\Omega\in\mathbb{P}(\mathcal{D})$ and a given function $\phi:\mathcal{D}\to\mathbb{R}^{d\times d}$, the notations ϕ^+ and ϕ^- denote the restrictions of ϕ to Ω and to $\mathcal{D}\backslash\overline{\Omega}$, respectively. If $\phi_1^+\in W^{1,1}(\Omega,\mathbb{R}^{d\times d})$ and $\phi_1^-\in W^{1,1}(\mathcal{D}\backslash\overline{\Omega},\mathbb{R}^{d\times d})$ then $[\![\phi]\!]:=\phi^+|_{\partial\Omega}-\phi^-|_{\partial\Omega}$ denotes the jump of the traces of ϕ across the interface $\partial\Omega$.

Notations. Let $\mathbf{S}:\mathbb{R}^d\to\mathbb{R}^{d\times d}$ be a second order tensor, then $\mathrm{div}(\mathbf{S})$ is defined as the vector of the divergence of the rows of $\mathbf{S}$.

Proposition 4.5. *Suppose that the conditions of theorem 4.3 are satisfied, and that* $V \in \mathcal{C}^1_c(\mathcal{D}\backslash\Gamma_h, \mathbb{R}^2)$*, then we have*

$$\mathrm{div}(\mathbf{S}_1^+) = (\mathbf{S}_0^r)^+ \quad a.e.\ in\ \Omega\backslash\Gamma_h, \tag{44}$$

$$\mathrm{div}(\mathbf{S}_1^-) = (\mathbf{S}_0^r)^- \quad a.e.\ in\ (\mathcal{D}\backslash\overline{\Omega})\backslash\Gamma_h. \tag{45}$$

If $\mathbf{S}_1^+ \in W^{1,1}(\Omega, \mathbb{R}^{2\times 2})$ *and* $\mathbf{S}_1^- \in W^{1,1}(\mathcal{D}\backslash\overline{\Omega}, \mathbb{R}^{2\times 2})$*, then*

$$dJ(\Omega)(V) = \int_\Omega \mathrm{div}(\mathbf{S}_1^\mathsf{T} V) + \int_{\mathcal{D}\backslash\overline{\Omega}} \mathrm{div}(\mathbf{S}_1^\mathsf{T} V). \tag{46}$$

If in addition Ω *is Lipschitz, we also have the boundary expression*

$$dJ(\Omega)(V) = \int_{\partial\Omega} [\![\mathbf{S}_1]\!] n \cdot V. \tag{47}$$

If in addition Ω *is of class* $\mathcal{C}^1$*, we obtain the boundary expression*

$$dJ(\Omega)(V) = \int_{\partial\Omega} ([\![\mathbf{S}_1]\!] n \cdot n)\, V \cdot n. \tag{48}$$

Proof. In view of [54, theorem 2.2], if V has compact support in Ω then the shape derivative vanishes. Assume $V \in \mathcal{C}^1_c(\Omega\backslash\Gamma_h, \mathbb{R}^2)$ and denote $U := \mathrm{supp} V \subset \Omega\backslash\Gamma_h$, then u and p are clearly harmonic in U since σ is constant in U. In view of (26) and the regularity of f_Ω, this yields $\mathbf{S}_1 \in L^1(U, \mathbb{R}^{2\mathrm{div}2})$ and $\mathrm{div}(\mathbf{S}_1) \in L^1(U, \mathbb{R}^2)$. Thus, we have $\mathrm{div}(\mathbf{S}_1^\mathsf{T} V) = \mathbf{S}_1 : DV + V \cdot \mathrm{div}(\mathbf{S}_1) \in L^1(U)$. For such V we also have $\mathbf{S}_0^s(V) = 0$, so we obtain

$$\begin{aligned} dJ(\Omega)(V) &= \mathbf{S}_0^s(V) + \int_{\mathcal{D}} \mathbf{S}_1 : DV + \mathbf{S}_0^r \cdot V \\ &= \int_U \mathrm{div}(\mathbf{S}_1^\mathsf{T} V) + V \cdot (\mathbf{S}_0^r - \mathrm{div}\mathbf{S}_1) = 0 \quad \text{for all} \quad V \in \mathcal{C}^1_c(\Omega\backslash\Gamma_h, \mathbb{R}^2). \end{aligned} \tag{49}$$

Since $\mathrm{supp} V = U \subset \Omega\backslash\Gamma_h$, we can extend $\mathbf{S}_1^\mathsf{T} V$ and $V \cdot (\mathbf{S}_0^r - \mathrm{div}\mathbf{S}_1)$ by zero on $\mathcal{B}$, where $\mathcal{B}$ is a sufficiently large open ball which contains U. We keep the same notation for the extensions for simplicity. Since the extension satisfies $\mathbf{S}_1^\mathsf{T} V \in W^{1,1}(\mathcal{B}, \mathbb{R}^2)$, using the divergence theorem (for instance [23, section 4.3, theorem 1]) in $\mathcal{B}$ we get

$$\begin{aligned} \int_U \mathrm{div}(\mathbf{S}_1^\mathsf{T} V) + V \cdot (\mathbf{S}_0^r - \mathrm{div}\mathbf{S}_1) &= \int_{\mathcal{B}} \mathrm{div}(\mathbf{S}_1^\mathsf{T} V) + V \cdot (\mathbf{S}_0^r - \mathrm{div}\mathbf{S}_1) \\ &= \int_{\partial\mathcal{B}} (\mathbf{S}_1^\mathsf{T} V) \cdot n + \int_{\mathcal{B}} V \cdot (\mathbf{S}_0^r - \mathrm{div}\mathbf{S}_1) \\ &= \int_\Omega V \cdot (\mathbf{S}_0^r - \mathrm{div}\mathbf{S}_1) = 0, \quad \text{for all} \quad V \in \mathcal{C}^1_c(\Omega\backslash\Gamma_h, \mathbb{R}^2), \end{aligned}$$

which proves (44). Then, we can prove (45) in a similar way by taking a vector $V \in \mathcal{C}^1_c((\mathcal{D}\backslash\overline{\Omega})\backslash\Gamma_h, \mathbb{R}^2)$.

Now, let us assume that $V \in \mathcal{C}^1_c(\mathcal{D}\backslash\Gamma_h, \mathbb{R}^2)$ and denote $U_2 := \mathrm{supp}\ V \subset \mathcal{D}\backslash\Gamma_h$. By standard elliptic regularity, we have $u \in H^1(U_2)$ and $p \in H^1(U_2)$. Assuming $\mathbf{S}_1^+ \in W^{1,1}(\Omega, \mathbb{R}^{2\times 2})$ and

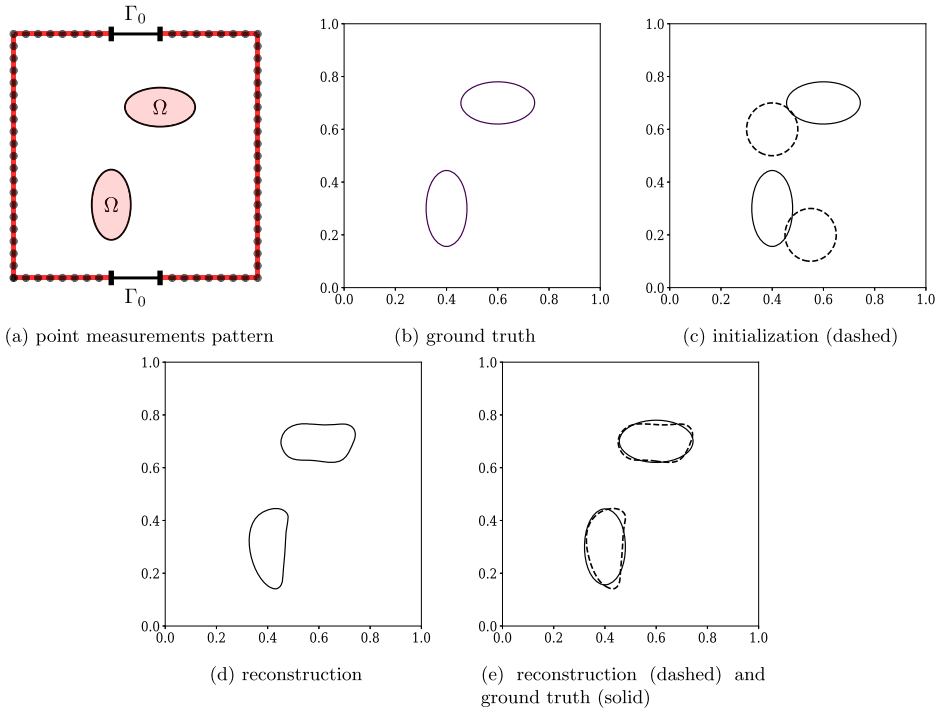

Figure 2. Reconstruction of two ellipses using $I = 3$ currents and $K = 70$ point measurements with 1.13% noise.

$\mathbf{S}_1^- \in W^{1,1}(\mathcal{D}\backslash\overline{\Omega}, \mathbb{R}^{2\times 2})$, and using (44) and (45) we obtain

$$\begin{aligned} dJ(\Omega)(V) &= \mathbf{S}_0(V) + \int_{\mathcal{D}} \mathbf{S}_1 : DV + \mathbf{S}_0^r \cdot V \\ &= \int_{\Omega} \mathbf{S}_1 : DV + \mathbf{S}_0^r \cdot V + \int_{\mathcal{D}\backslash\overline{\Omega}} \mathbf{S}_1 : DV + \mathbf{S}_0^r \cdot V \\ &= \int_{\Omega} \operatorname{div}(\mathbf{S}_1^{\mathsf{T}} V) + V \cdot (\mathbf{S}_0^r - \operatorname{div}\mathbf{S}_1) + \int_{\mathcal{D}\backslash\overline{\Omega}} \operatorname{div}(\mathbf{S}_1^{\mathsf{T}} V) + V \cdot (\mathbf{S}_0^r - \operatorname{div}\mathbf{S}_1) \\ &= \int_{\Omega} \operatorname{div}(\mathbf{S}_1^{\mathsf{T}} V) + \int_{\mathcal{D}\backslash\overline{\Omega}} \operatorname{div}(\mathbf{S}_1^{\mathsf{T}} V), \end{aligned}$$

which yields (46). If in addition Ω is Lipschitz, applying the divergence theorem to (46) we get (47).

In view of (47), we have that $dJ(\Omega)$ is continuous for the $\mathcal{C}^0(\mathcal{D}, \mathbb{R}^d)$-topology. Thus, if Ω is of class $\mathcal{C}^1$, we can apply theorem 4.4 with $k = 0$. If Ω is of class $\mathcal{C}^1$, we also have $n \in \mathcal{C}^0(\partial\Omega, \mathbb{R}^2)$ and $(V_{|\partial\Omega} \cdot n)n \in \mathcal{C}^0(\partial\Omega, \mathbb{R}^2)$. Let $\hat{V} \in \mathcal{C}_c^0(\mathcal{D}\backslash\Gamma_h, \mathbb{R}^2)$ be an extension of $(V_{|\partial\Omega} \cdot n)n$, then using theorem 4.4 and (47) we obtain

$$\begin{aligned} dJ(\Omega)(V) &= l(V_{|\partial\Omega} \cdot n) = l(\hat{V}_{|\partial\Omega} \cdot n) = dJ(\Omega)(\hat{V}) \\ &= \int_{\partial\Omega} ((\mathbf{S}_1^+ - \mathbf{S}_1^-)n) \cdot \hat{V} = \int_{\partial\Omega} ([\![\mathbf{S}_1]\!]n) \cdot ((V \cdot n)n) = \int_{\partial\Omega} ([\![\mathbf{S}_1]\!]n \cdot n)V \cdot n, \end{aligned}$$

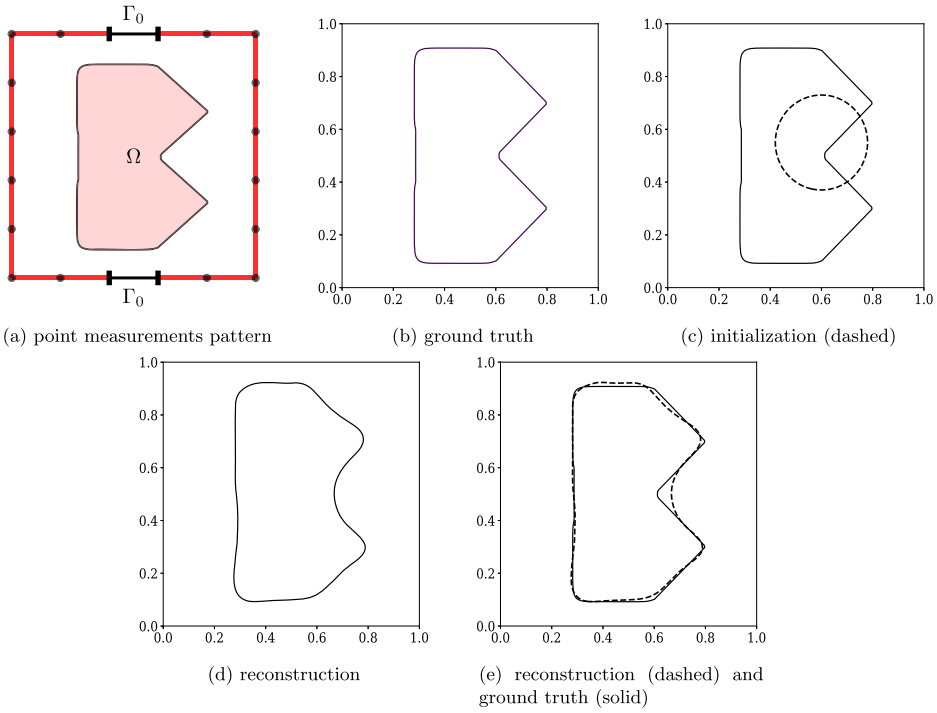

Figure 3. Reconstruction of a concave shape using $I = 3$ currents and $K = 34$ point measurements with 0.55% noise.

which yields expression (48). □

Remark 4.6. Proposition 4.5 is in fact valid for any shape functional whose distributed shape derivative can be written using a tensor expression of the type (25), and which satisfies appropriate regularity assumptions. Note that in general, one should not expect that the assumption $\mathbf{S}_1^+ \in W^{1,1}(\Omega, \mathbb{R}^{2\times 2})$ and $\mathbf{S}_1^- \in W^{1,1}(\mathcal{D}\backslash\overline{\Omega}, \mathbb{R}^{2\times 2})$ in proposition 4.5 can be satisfied for any Lipschitz set Ω. For instance in the case of the Dirichlet Laplacian, one can actually build pathological Lipschitz domains for which $\mathbf{S}_1$ does not have such regularity; see [17, corollary 3.2]. However, these regularity assumptions for $\mathbf{S}_1^+, \mathbf{S}_1^-$ can be fulfiled for polygonal domains, as shown in corollary 4.7.

Corollary 4.7. *Suppose that the conditions of theorem 4.3 are satisfied, and that in addition $f_0 \in \mathcal{C}^\infty(\mathcal{D})$ and $V \in \mathcal{C}_c^1(\mathcal{D}\backslash\Gamma_h, \mathbb{R}^2)$. If Ω is Lipschitz polygonal or if Ω is of class $\mathcal{C}^1$, then we have*

$$dJ(\Omega)(V) = \int_{\partial\Omega} ([\![\sigma_\Omega \partial_n u \partial_n p]\!] + [\![\sigma_\Omega]\!]\nabla_{\partial\Omega} u \cdot \nabla_{\partial\Omega} p - [\![f_\Omega]\!]p)V \cdot n, \tag{50}$$

where $\nabla_{\partial\Omega}$ denotes the tangential gradient on $\partial\Omega$.

Proof. In the case where Ω is of class $\mathcal{C}^1$, a quick calculation using (48) and (26) yields (50).

In the case where Ω is polygonal, we can proceed in the following way. Let $\widehat{\mathcal{D}}$ be a smooth open set such that supp $V \cup \overline{\Omega} \subset \widehat{\mathcal{D}} \subset \mathcal{D}$ and the boundaries of Ω and $\widehat{\mathcal{D}}$ are at a positive distance. Since $f_0 \in \mathcal{C}^\infty(\mathcal{D})$, using elliptic regularity we get that u and p are $\mathcal{C}^\infty$ on $\partial\widehat{\mathcal{D}}$. Thus, $u|_{\widehat{\mathcal{D}}}$

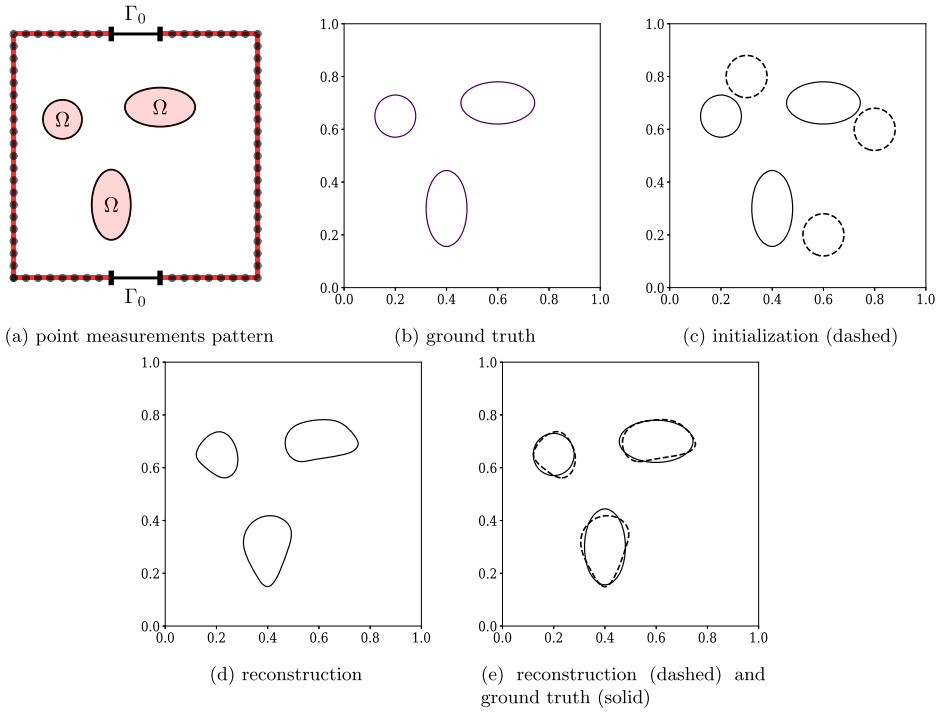

Figure 4. Reconstruction of three ellipses using $I = 7$ currents and $K = 70$ point measurements with 0.63% noise.

and $p|_{\widehat{\mathcal{D}}}$ are also solutions of transmission problems defined in $\widehat{\mathcal{D}}$ with smooth inhomogeneous Dirichlet conditions on $\partial\widehat{\mathcal{D}}$, and consequently we are in the framework considered in [57]. Denote L the number of vertices of the polygon Ω. We apply [57, theorem 7.3] in the case $k = 0$, $m = 1$ and for the regularity $W^{2,4/3}$. This yields the decomposition $u|_{\widehat{\mathcal{D}}} = u_0 + \sum_{\ell\in L} S_\ell$ with $u_0^+ \in W^{2,4/3}(\Omega)$, $u_0^- \in W^{2,4/3}(\widehat{\mathcal{D}}\backslash\overline{\Omega})$ and S_ℓ are singular functions with support in the neighbourhood of the vertices of Ω. Here $S_\ell(r_\ell, \theta_\ell)$ are of the type $r_\ell^{\lambda_\ell} v(r_\ell, \theta_\ell)$, where (r_ℓ, θ_ℓ) are local polar coordinates at the vertex ℓ and $v(\theta_\ell)$ is a linear combination of $\sin(\lambda_\ell\theta_\ell)$ and $\cos(\lambda_\ell\theta_\ell)$. It is shown in [18, theorem 8.1(ii)] that $\lambda_\ell > 1/2$ for all $\ell = 1, \ldots, L$. Thus, we also obtain $\sum_{\ell\in L} S_\ell^+ \in W^{2,4/3}(\Omega)$ and $\sum_{\ell\in L} S_\ell^- \in W^{2,4/3}(\widehat{\mathcal{D}}\backslash\overline{\Omega})$.

Proceeding in a similar way for p and gathering the results, we obtain the regularity u^+, $p^+ \in W^{2,4/3}(\Omega)$ and $u^-, p^- \in W^{2,4/3}(\widehat{\mathcal{D}}\backslash\overline{\Omega})$. Then we have $\nabla(\nabla u \cdot \nabla p) = (D^2u)p + (D^2p)u$ and using $(D^2u)^+, (D^2p)^+ \in L^{4/3}(\Omega)$ and $(\nabla u)^+, (\nabla p)^+ \in W^{1,4/3}(\Omega) \subset L^4(\Omega)$ and the same regularity on $\widehat{\mathcal{D}}\backslash\overline{\Omega}$, we obtain $\mathbf{S}_1^+ \in W^{1,1}(\Omega, \mathbb{R}^{2\times 2})$ and $\mathbf{S}_1^- \in W^{1,1}(\widehat{\mathcal{D}}\backslash\overline{\Omega}, \mathbb{R}^{2\times 2})$.

Then, using the fact that $V \in \mathcal{C}_c^1(\mathcal{D}\backslash\Gamma_h, \mathbb{R}^2)$ we obtain in view of (47) of proposition 4.5

$$dJ(\Omega)(V) = \int_{\partial\Omega} [\![\sigma_\Omega \partial_n u]\!] \nabla_{\partial\Omega} u \cdot V + [\![\sigma_\Omega \partial_n p]\!] \nabla_{\partial\Omega} p \cdot V + \int_{\partial\Omega} ([\![\sigma_\Omega \partial_n u \partial_n p]\!] + [\![\sigma_\Omega]\!] \nabla_{\partial\Omega} u \cdot \nabla_{\partial\Omega} p - [\![f_\Omega]\!] p) V \cdot n.$$

Finally, using the fact that $[\![\sigma_\Omega \partial_n u]\!] = 0$ and $[\![\sigma_\Omega \partial_n p]\!] = 0$ we obtain (50). □

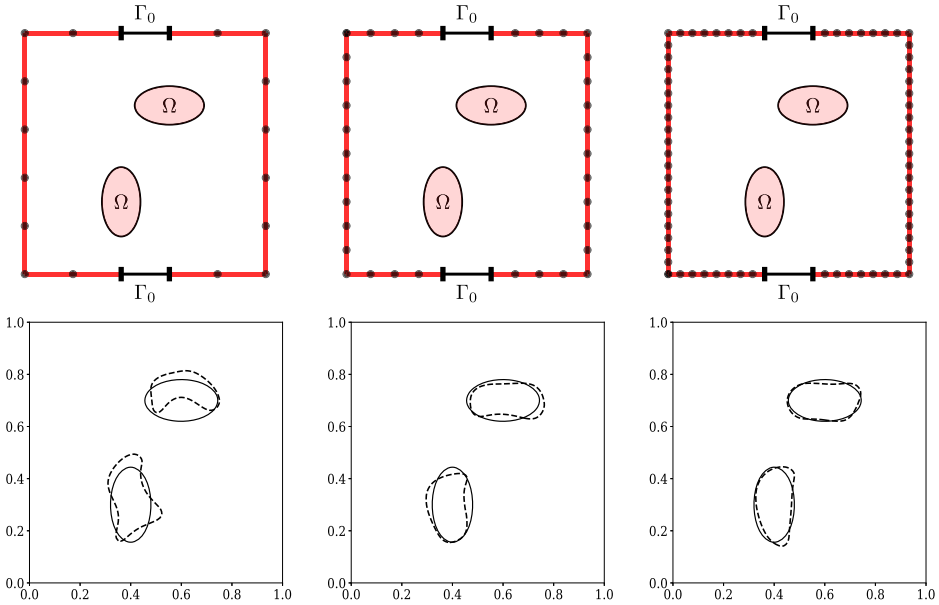

(a) $K = 16$ point measurements, 1.18% noise, 54.00% relative error

(b) $K = 34$ point measurements, 1.18% noise, 27.13% relative error

(c) $K = 70$ point measurements, 1.13% noise, 17.19% relative error

Figure 5. Reconstruction of two ellipses using $I = 3$ currents and three different sets of point measurements shown in the first row.

Remark 4.8. Expressions similar to (50) are known when Ω is at least $\mathcal{C}^1$, see [2, 54]. It is remarkable that one obtains the same expression (50) when Ω is only Lipschitz polygonal. Also, note that (50) is similar to the formula obtained in [9] for a polygonal inclusion in EIT, which was obtained in the framework of the perturbation of identity method. In [9], an estimate of the singularity of the gradient in the neighbourhood of the vertices of the polygonal inclusion was used to obtain the boundary expression. Here, we have used higher regularity of u and p in the subdomains Ω and $\widehat{\mathcal{D}}\backslash\overline{\Omega}$ to obtain (50). The core idea of these two approaches is to control the singularity of the gradients of u and p near the vertices of the polygonal inclusion.

5. Numerical experiments

We use the software package FEniCS for the implementation; see [4, 53, 55]. For the numerical tests the conductivity values are set to $\sigma_0 = 1$ and $\sigma_1 = 10$. We choose $f_\Omega \equiv 0$, $\mathcal{D} = (0,1) \times (0,1)$ and

$$\Gamma = \partial D \backslash ([0.4, 0.6] \times \{0\} \cup [0.4, 0.6] \times \{1\}).$$

The domain $\mathcal{D}$ is meshed using a regular grid of 128×128 elements. For the measurement points we choose $\Gamma_h = \{x_k\}_{k=1}^K \subset \Gamma$. Recall that no measurements are performed on $\Gamma_0 = \partial\mathcal{D}\backslash\Gamma$ and that u satisfies Dirichlet boundary condition on Γ_0.

Synthetic measurements $\{h_i(x_k)\}_{k=1}^K$ are obtained by taking the trace on Γ of the solution of (9) using the ground truth domain denoted by $\Omega^\star$, $f_{\Omega^\star} \equiv 0$ and currents g_i, $i = 1, \ldots, I$. To simulate noisy EIT data, each measurement h_i is corrupted by adding a normal Gaussian noise

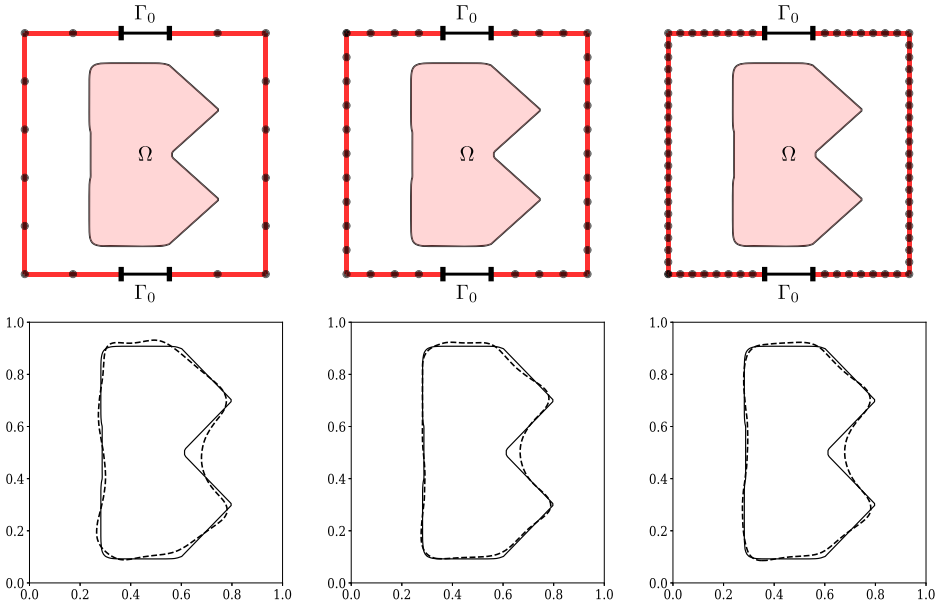

(a) $K = 16$ point measurements, 0.50% noise, 8.81% relative error

(b) $K = 34$ point measurements, 0.55% noise, 5.28% relative error

(c) $K = 70$ point measurements, 0.58% noise, 6.77% relative error

Figure 6. Reconstruction of a concave shape using $I = 3$ currents and three different sets of point measurements shown in the first row.

with mean zero and standard deviation $\delta * \|h_i\|_\infty$, where δ is a parameter. The noise level is then computed as

$$\text{noise} = \frac{\sum_{i=1}^{I} (\sum_{k=1}^{K} |h_i(x_k) - \tilde{h}_i(x_k)|^2)^{1/2}}{\sum_{i=1}^{I} (\sum_{k=1}^{K} |h_i(x_k)|^2)^{1/2}}, \tag{51}$$

where $h_i(x_k)$ and $\tilde{h}_i(x_k)$ are respectively the noiseless and noisy point measurements at x_k corresponding to the current g_i.

In the numerical tests, we use two different sets of fluxes, i.e. $I \in \{3, 7\}$, to obtain measurements. Denote Γ_{upper}, Γ_{lower}, Γ_{left} and Γ_{right} the four sides of the square D. When $I = 3$ we take

$$\begin{aligned} g_1 &= 1 \text{ on } \Gamma_{\text{left}} \cup \Gamma_{\text{right}} \quad \text{and} \quad g_1 = -1 \text{ on } \Gamma_{\text{upper}} \cup \Gamma_{\text{lower}}, \\ g_2 &= 1 \text{ on } \Gamma_{\text{left}} \cup \Gamma_{\text{upper}} \quad \text{and} \quad g_2 = -1 \text{ on } \Gamma_{\text{right}} \cup \Gamma_{\text{lower}}, \\ g_3 &= 1 \text{ on } \Gamma_{\text{left}} \cup \Gamma_{\text{lower}} \quad \text{and} \quad g_3 = -1 \text{ on } \Gamma_{\text{right}} \cup \Gamma_{\text{upper}}. \end{aligned}$$

When $I = 7$ we take in addition a smooth approximation of the following piecewise constant function:

$$g_4 = 1 \text{ on } \Gamma_{\text{left}} \cap \{x_2 > 0.5\}, \quad g_4 = -1 \text{ on } \Gamma_{\text{left}} \cap \{x_2 \leqslant 0.5\} \quad \text{and} \quad g_4 = 0 \quad \text{otherwise},$$

and g_5, g_6, g_7 are defined in a similar way on Γ_{right}, Γ_{upper}, Γ_{lower}, respectively.

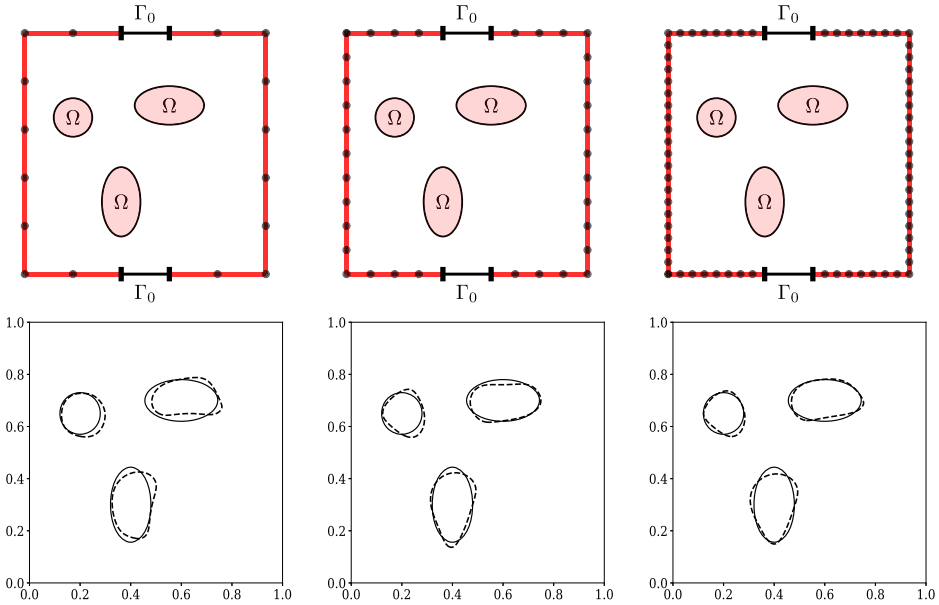

(a) $K = 16$ point measurements, 0.59% noise, 25.52% relative error

(b) $K = 34$ point measurements, 0.54% noise, 18.8% relative error

(c) $K = 70$ point measurements, 0.63% noise, 16.1% relative error

Figure 7. Reconstruction of three ellipses using $I = 7$ currents and different sets of point measurements shown in the first row.

For the numerics we use the cost functional given by (5):

$$J(\Omega) = \frac{1}{2}\sum_{i=1}^{I} \mu_i \sum_{k=1}^{K} (u_i(x_k) - h_i(x_k))^2, \tag{52}$$

where u_i is the potential associated with the current g_i. The weights μ_i associated with the current g_i are chosen as the inverse of $\sum_{k=1}^{K} (u_i(x_k) - h_i(x_k))^2$ computed at the initial guess. In this way, each term in the sum over $i = 1, \ldots, I$, is equal to 1 at the first iteration, and the initial value of $J(\Omega)$ is equal to $I/2$.

To get a relatively smooth descent direction we solve the following partial differential equation: find $V \in H_0^1(\mathcal{D}, \mathbb{R}^2)$ such that

$$\int_{\mathcal{D}} \alpha_1 DV : D\xi + \alpha_2 V \cdot \xi = -dJ(\Omega)(\xi) \quad \text{for all} \quad \xi \in H_0^1(\mathcal{D}, \mathbb{R}^2). \tag{53}$$

Supposing $V \neq 0$ and choosing $\xi = V$ in (53), we obtain

$$dJ(\Omega)(V) = -\int_{\mathcal{D}} \alpha_1 DV : DV + \alpha_2 V \cdot V < 0,$$

which shows that the solution V of (53) is a descent direction for J. The regularity of the reconstructed shape can be controlled via the coefficient $\alpha_1 > 0$: a larger ratio α_1/α_2 yields a smoother reconstruction. For the numerical tests, we have found that the heuristic values $\alpha_1 = 0.3$ and $\alpha_2 = 0.7$ give good results.

To simplify the implementation, we use Dirichlet conditions on $\partial\mathcal{D}$ instead of the compact support condition $V \in \mathcal{C}_c^1(\mathcal{D}\backslash\Gamma_h, \mathbb{R}^2)$ (see section 4). Considering that $f_\Omega \equiv 0$ in $\mathcal{D}$, $V = 0$ on

Table 1. Influence of noise and number of point measurements on the reconstruction of two ellipses using $I = 3$ currents (the noise value is the average over the noise values for the three levels of point measurements).

Noise (%)	$K = 16$ points	$K = 34$ points	$K = 70$ points
0%	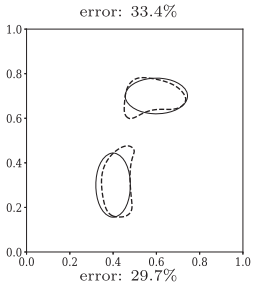	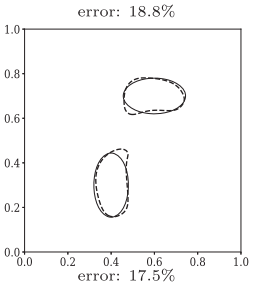	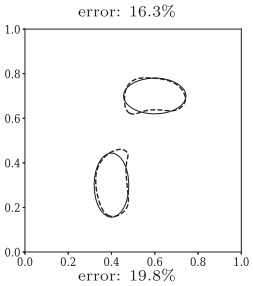
0.51%	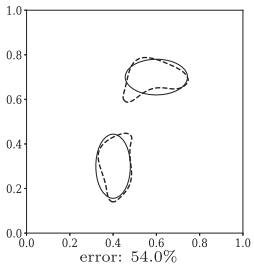	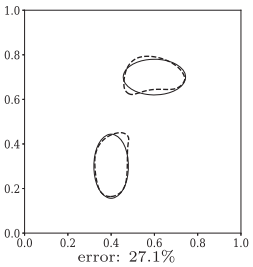	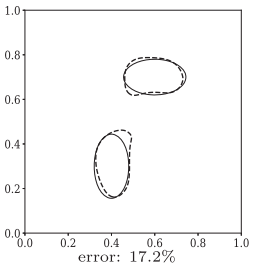
1.16%	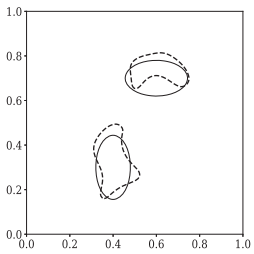	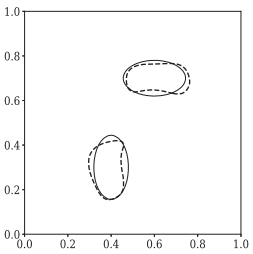	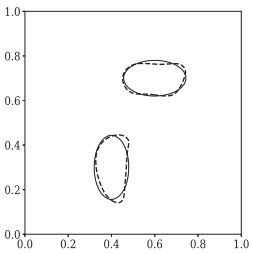

$\partial\mathcal{D}$ and that the points $\{x_k\}_{k=1}^K$ belong to Γ, in view of theorem 4.3 we get $\mathbf{S}_0^s(V) = 0$ which leads to the following equation for V:

$$\int_{\mathcal{D}} \alpha_1 DV : D\xi + \alpha_2 V \cdot \xi$$
$$= -\int_{\mathcal{D}} - 2\sigma_\Omega(\nabla u \odot \nabla p) : D\xi + (\sigma_\Omega \nabla u \cdot \nabla p)\mathbb{I} : D\xi \quad \text{for all } \xi \in H_0^1(\mathcal{D}, \mathbb{R}^2).$$

The relative reconstruction error $E(\Omega^r)$ is defined as

$$E(\Omega^r) := \frac{\int_{\mathcal{D}} |\chi_{\Omega^\star} - \chi_{\Omega^r}|}{\int_{\mathcal{D}} \chi_{\Omega^\star}},$$

where Ω^r is the set obtained in the last iteration of the minimization algorithm. We use $E(\Omega^r)$ as a measure of the quality of the reconstructions.

We present three numerical experiments. In the first experiment, the ground truth consists of two ellipses and we use $I = 3$ currents; see figure 2. In the second experiment, the ground truth is a concave shape with one connected component and we use $I = 3$ currents; see figure 3.

Table 2. Influence of noise and number of point measurements on the reconstruction of a concave shape using $I = 3$ currents (the noise value is the average over the noise values for the three levels of point measurements).

Noise (%)	$K = 16$ points	$K = 34$ points	$K = 70$ points
0%	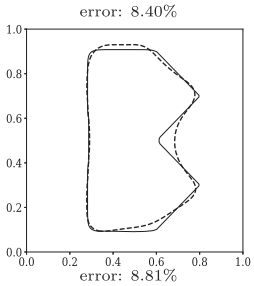	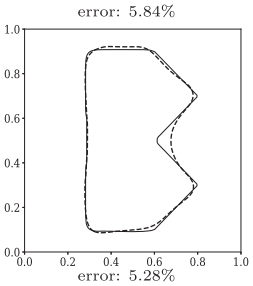	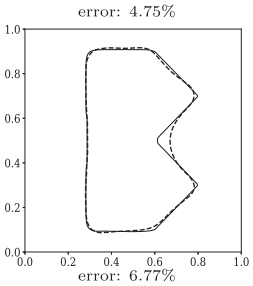
0.54%	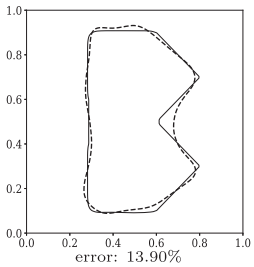	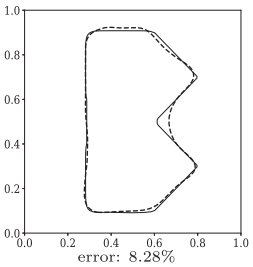	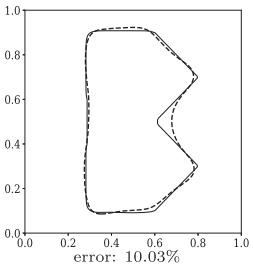
1.12%	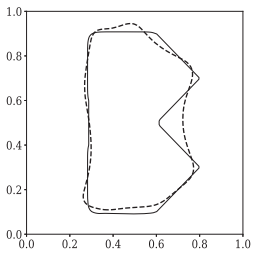	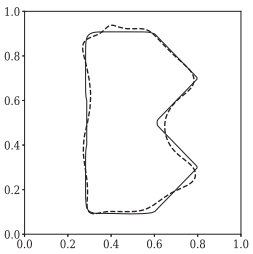	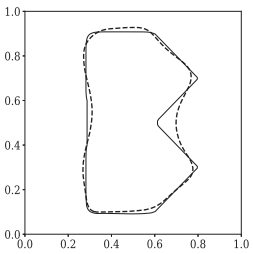

In the third experiment, the ground truth consists of two ellipses and one ball and we use $I = 7$ currents; see figure 4. For each experiment, we study the influence of the point measurements patterns by comparing the reconstructions obtained using three different sets $\Gamma_h = \{x_k\}_{k=1}^K$ with $K \in \{16, 34, 70\}$. The point measurements patterns and the corresponding reconstructions are presented in figures 5–7, for the respective experiments. We observe, as expected, that the reconstructions improve as K becomes larger. However, one obtains reasonable reconstructions in the case of the concave shape with $I = 3$ currents and in the case of the two ellipses and ball with $I = 7$ currents, even for $K = 16$ points and in the presence of noise; see figures 6 and 7. In the case of two ellipses, the deterioration of the reconstruction for $K = 16$ points is much stronger compared to the case $K = 70$. This indicates that the number of currents $I = 3$ is too low to reconstruct two ellipses with only $K = 16$ points. We conclude from these results that the number of applied currents is more critical than the number of point measurements to obtain a good reconstruction.

For each experiment, we also study how the noise level affects the reconstruction depending on the number of point measurements. The results are gathered in tables 1–3, where the rows correspond to three different levels of noise, and the columns to three different numbers of points $K \in \{16, 34, 70\}$. In the case of two ellipses (table 1), the reconstruction using $K = 70$

Table 3. Influence of noise and number of point measurements on the reconstruction of three ellipses using $I = 7$ currents (the noise value is the average over the noise values for the three levels of point measurements).

Noise (%)	$K = 16$ points	$K = 34$ points	$K = 70$ points
0%	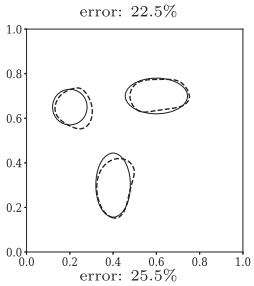	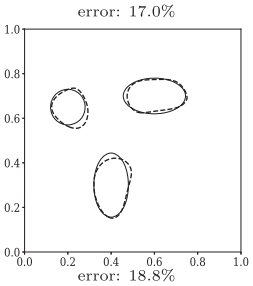	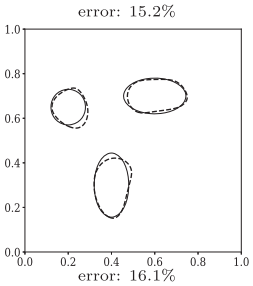
0.59%	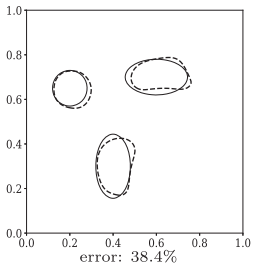	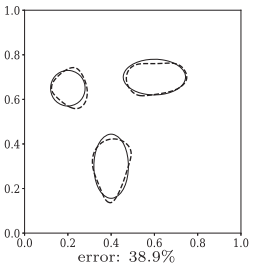	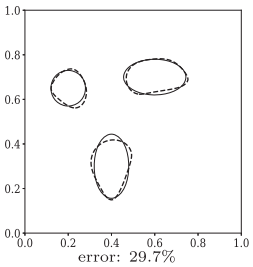
1.14%	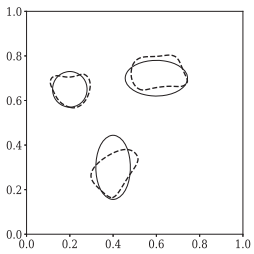	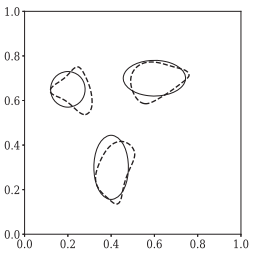	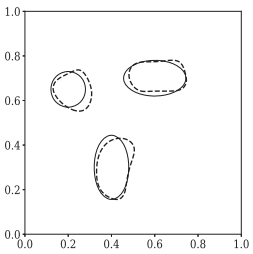

is very robust with respect to noise, whereas it deteriorates considerably using $K = 16$. In the cases of the concave shape (table 2) and of the two ellipses and ball (table 3), the degradations of the reconstructions when the noise becomes larger are of a similar order in terms of reconstruction error, independently of the value of K. These results indicate that a larger number of points K may improve the robustness of the reconstruction with respect to noise mainly when the number I of currents is low compared to the complexity of the ground truth.

Acknowledgments

The authors would like to thank the reviewers for their useful comments which helped improve the paper. Yuri Flores Albuquerque and Antoine Laurain gratefully acknowledge support of the RCGI—Research Centre for Gas Innovation, hosted by the University of São Paulo (USP) and sponsored by FAPESP—São Paulo Research Foundation (2014/50279-4) and Shell Brasil. This research was carried out in association with the ongoing R & D project registered as ANP 20714-2—Desenvolvimento de técnicas numéricas e software para problemas de inversão com aplicações em processamento sísmico (USP/Shell Brasil/ANP), sponsored

by Shell Brasil under the ANP R & D levy as 'Compromisso de Investimentos com Pesquisa e Desenvolvimento'. Antoine Laurain gratefully acknowledges the support of FAPESP, process: 2016/24776-6 'Otimização de forma e problemas de fronteira livre', and of the Brazilian National Council for Scientific and Technological Development (Conselho Nacional de Desenvolvimento Científico e Tecnológico—CNPq) through the process: 408175/2018-4 'Otimização de forma não suave e controle de problemas de fronteira livre', and through the programme 'Bolsa de Produtividade em Pesquisa—PQ 2015', process: 304258/2018-0.

Appendix. Averaged adjoint method

In this appendix we describe the averaged adjoint method introduced in [64], see also [54]. Let $t_0 > 0$ be given and $E = E(\mathcal{D}), F = F(\mathcal{D})$ be two Banach spaces, and consider a parameterization $\Omega_t = T_t(\Omega)$ for $t \in [0, t_0]$ such that $T_t(\mathcal{D}) = \mathcal{D}$, i.e. which leaves $\mathcal{D}$ globally invariant. Our goal is to differentiate shape functions of the type $J(\Omega_t)$ which can be written using a Lagrangian as $J(\Omega_t) = \mathcal{L}(\Omega_t, u^t, \hat{\psi})$, where $u^t \in E(\mathcal{D})$ and $\hat{\psi} \in F(\mathcal{D})$. The main appeal of the Lagrangian is that we actually only need to compute the partial derivative with respect to t of $\mathcal{L}(\Omega_t, \hat{\varphi}, \hat{\psi})$ to compute the derivative of $J(\Omega_t)$, indeed this is the main result of theorem 6.3.

In order to differentiate $\mathcal{L}(\Omega_t, \hat{\varphi}, \hat{\psi})$, the change of coordinates $x \mapsto T_t(x)$ is used in the integrals. In the process appear the pullbacks $\hat{\varphi} \circ T_t \in E(\mathcal{D})$ and $\hat{\psi} \circ T_t \in F(\mathcal{D})$ which depend on t. The usual procedure in shape optimization to compensate this effect is to use a reparameterization $\mathcal{L}(\Omega_t, \Psi_t(\varphi), \Psi_t(\psi))$ instead of $\mathcal{L}(\Omega_t, \hat{\varphi}, \hat{\psi})$, where Ψ_t is an appropriate bijection of $E(\mathcal{D})$ and $F(\mathcal{D})$, and $\varphi \in E(\mathcal{D})$, $\psi \in F(\mathcal{D})$. Now the change of variable in the integrals yields functions φ and ψ in the integrands, which are independent of t. In this paper we take $E(\mathcal{D}) = W^1_{\Gamma,q}(\mathcal{D})$, $F(\mathcal{D}) = W^1_{\Gamma,q'}(\mathcal{D})$, and $\Psi_t(\psi) = \psi \circ T_t^{-1}$ is then a bijection of $E(\mathcal{D})$ and $F(\mathcal{D})$; see [68, theorem 2.2.2, p 52].

Thus we consider the so-called *shape-Lagrangian* $G : [0, t_0] \times E \times F \to \mathbb{R}$ with

$$G(t, \varphi, \psi) := \mathcal{L}(\Omega_t, \varphi \circ T_t^{-1}, \psi \circ T_t^{-1}).$$

The main result of this section, theorem 6.3, shows that in order to obtain the shape derivative of $\mathcal{L}$, it is enough to compute the partial derivative with respect to t of G while assigning the values $\varphi = u$ and $\psi = p$, where u is the state and p is the adjoint state. The main ingredient is the introduction of the averaged adjoint equation described below.

Let us assume that for each $t \in [0, t_0]$ the equation

$$d_\psi G(t, u^t, 0; \hat{\psi}) = 0 \quad \text{for all} \quad \hat{\psi} \in F, \tag{54}$$

admits a unique solution $u^t \in E$. Further, we make the following assumptions for G.

Assumption 6.1. For every $(t, \psi) \in [0, t_0] \times F$

(a) $[0, 1] \ni s \mapsto G(t, su^t + (1 - s)u^0), \psi)$ is absolutely continuous.
(b) $[0, 1] \ni s \mapsto d_\varphi G(t, su^t + (1 - s)u^0, \psi; \hat{\varphi})$ belongs to $L^1(0, 1)$ for all $\hat{\varphi} \in E$.

When assumption 6.1 is satisfied, for $t \in [0, t_0]$ we introduce the *averaged adjoint equation* associated with u^t and u^0: find $p^t \in F$ such that

$$\int_0^1 d_\varphi G(t, su^t + (1 - s)u^0, p^t; \hat{\varphi}) \, \mathrm{d}s = 0 \quad \text{for all} \quad \hat{\varphi} \in E. \tag{55}$$

In view of assumption 6.1 we have

$$G(t,u^t,p^t)-G(t,u^0,p^t)=\int_0^1 d_\varphi G(t,su^t+(1-s)u^0,p^t;u^t-u^0)\,\mathrm{d}s=0 \quad \text{for all} \quad t\in[0,t_0]. \tag{56}$$

We can now state the main result of this section.

Assumption 6.2. We assume that

$$\lim_{t\searrow 0}\frac{G(t,u^0,p^t)-G(0,u^0,p^t)}{t}=\partial_t G(0,u^0,p^0).$$

Theorem 6.3. *Let assumptions 6.1 and 6.2 be satisfied and assume there exists a unique solution p^t of the averaged adjoint equation (55). Then for all $\psi\in F$ we obtain*

$$\mathrm{dt}(G(t,u^t,\psi))|_{t=0}=\partial_t G(0,u^0,p^0). \tag{57}$$

ORCID iDs

Yuri Flores Albuquerque https://orcid.org/0000-0002-8495-5511
Antoine Laurain https://orcid.org/0000-0002-8733-5190
Kevin Sturm https://orcid.org/0000-0001-9855-739X

References

[1] Adams R A and Fournier J J F 2003 *Sobolev Spaces* (Pure and Applied Mathematics vol 140) 2nd edn (Amsterdam: Elsevier/Academic)
[2] Afraites L, Dambrine M and Kateb D 2007 Shape methods for the transmission problem with a single measurement *Numer. Funct. Anal. Optim.* **28** 519–51
[3] Afraites L, Dambrine M and Kateb D 2008 On second order shape optimization methods for electrical impedance tomography *SIAM J. Control Optim.* **47** 1556–90
[4] Alnæs M *et al* 2015 The fenics project version 1.5 *Archive of Numerical Software* **3** 9–23
[5] Alsaker M, Hamilton S J and Hauptmann A 2017 A direct D-bar method for partial boundary data electrical impedance tomography with *a priori* information *Inverse Problems Imaging* **11** 427–54
[6] Ammari H, Garnier J, Jugnon V and Kang H 2012 Stability and resolution analysis for a topological derivative based imaging functional *SIAM J. Control Optim.* **50** 48–76
[7] Ammari H and Kang H 2004 *Reconstruction of Small Inhomogeneities from Boundary Measurements* (Lecture Notes in Mathematics vol 1846) (Berlin: Springer)
[8] Bera T K 2018 Applications of electrical impedance tomography (EIT): a short review *IOP Conf. Ser.: Mater. Sci. Eng.* **331** 012004
[9] Beretta E, Micheletti S, Perotto S and Santacesaria M 2018 Reconstruction of a piecewise constant conductivity on a polygonal partition via shape optimization in EIT *J. Comput. Phys.* **353** 264–80
[10] Berggren M 2010 A unified discrete-continuous sensitivity analysis method for shape optimization *Applied and Numerical Partial Differential Equations* (Computing Methods in Applied Sciences vol 15) (New York: Springer) pp 25–39
[11] Bonnet M 2009 Higher-order topological sensitivity for 2-D potential problems. Application to fast identification of inclusions *Internat. J. Solids Structures* **46** 2275–92
[12] Borcea L 2002 Electrical impedance tomography *Inverse Problems* **18** R99–136
[13] Borcea L, Druskin V and Mamonov A V 2010 Circular resistor networks for electrical impedance tomography with partial boundary measurements *Inverse Problems* **26** 045010
[14] Brühl M and Hanke M 2000 Numerical implementation of two noniterative methods for locating inclusions by impedance tomography *Inverse Problems* **16** 1029–42

[15] Chesnel L, Hyvönen N and Staboulis S 2015 Construction of indistinguishable conductivity perturbations for the point electrode model in electrical impedance tomography *SIAM J. Appl. Math.* **75** 2093–109
[16] Chung E T, Chan T F and Tai X-C 2005 Electrical impedance tomography using level set representation and total variational regularization *J. Comput. Phys.* **205** 357–72
[17] Costabel M 2019 On the limit sobolev regularity for Dirichlet and Neumann problems on Lipschitz domains *Mathematische Nachrichten* **292** 2165–73
[18] Costabel M, Dauge M and Nicaise S 1999 Singularities of Maxwell interface problems *M2AN Math. Model. Numer. Anal.* **33** 627–49
[19] de Castro Martins T *et al* 2019 A review of electrical impedance tomography in lung applications: Theory and algorithms for absolute images *Annual Reviews in Control* **48** 442–71
[20] Delfour M, Payre G and Zolésio J-P 1985 An optimal triangulation for second-order elliptic problems *Comput. Methods Appl. Mech. Eng.* **50** 231–61
[21] Delfour M C and Zolésio J-P 2011 *Shapes and Geometries: Metrics, Analysis, Differential Calculus, and Optimization* (Advances in Design and Control vol 22) 2nd edn (Philadelphia, PA: Society for Industrial and Applied Mathematics (SIAM))
[22] Eckel H and Kress R 2007 Nonlinear integral equations for the inverse electrical impedance problem *Inverse Problems* **23** 475–91
[23] Evans L C and Gariepy R F 1992 Measure theory and fine properties of functions *Studies in Advanced Mathematics* (Boca Raton, FL: CRC Press)
[24] Friedman A 1987 Detection of mines by electric measurements *SIAM J. Appl. Math.* **47** 201–12
[25] Friedman A and Isakov V 1989 On the uniqueness in the inverse conductivity problem with one measurement *Indiana Univ. Math. J.* **38** 563–79
[26] Garde H and Knudsen K 2015 3D reconstruction for partial data electrical impedance tomography using a sparsity prior *Discrete Contin. Dyn. Syst.*, (*Dynamical Systems, Differential Equations and Applications. 10th AIMS Conference. Suppl.*) pp 495–504
[27] Garde H and Knudsen K 2016 Sparsity prior for electrical impedance tomography with partial data *Inverse Probl. Sci. Eng.* **24** 524–41
[28] Garde H and Staboulis S 2017 Convergence and regularization for monotonicity-based shape reconstruction in electrical impedance tomography *Numer. Math.* **135** 1221–51
[29] Giacomini M, Pantz O and Trabelsi K 2017 Certified descent algorithm for shape optimization driven by fully-computable *a posteriori* error estimators *ESAIM Control Optim. Calc. Var.* **23** 977–1001
[30] Gröger K 1989 A $W^{1,p}$-estimate for solutions to mixed boundary value problems for second order elliptic differential equations *Math. Ann.* **283** 679–87
[31] Gröger K and Rehberg J 1989 Resolvent estimates in $W^{-1,p}$ for second order elliptic differential operators in case of mixed boundary conditions *Math. Ann.* **285** 105–13
[32] Haller-Dintelmann R, Meyer C, Rehberg J and Schiela A 2009 Hölder continuity and optimal control for nonsmooth elliptic problems *Appl. Math. Optim.* **60** 397–428
[33] Hanke M, Harrach B and Hyvönen N 2011 Justification of point electrode models in electrical impedance tomography *Math. Models Methods Appl. Sci.* **21** 1395–413
[34] Harrach B 2013 Recent progress on the factorization method for electrical impedance tomography *Comput. Math. Methods Med.* **8** 425184
[35] Harrach B and Minh M N 2016 Enhancing residual-based techniques with shape reconstruction features in electrical impedance tomography *Inverse Problems* **32** 125002
[36] Harrach B and Ullrich M 2013 Monotonicity-based shape reconstruction in electrical impedance tomography *SIAM J. Math. Anal.* **45** 3382–403
[37] Haug E J, Choi K K and Komkov V 1986 *Design Sensitivity Analysis of Structural Systems* (Mathematics in Science and Engineering vol 177) (New York: Academic)
[38] Hauptmann A, Santacesaria M and Siltanen S 2017 Direct inversion from partial-boundary data in electrical impedance tomography *Inverse Problems* **33** 025009
[39] Hettlich F and Rundell W 1998 The determination of a discontinuity in a conductivity from a single boundary measurement *Inverse Problems* **14** 67–82
[40] Hintermüller M and Laurain A 2008 Electrical impedance tomography: from topology to shape *Control Cybernet* **37** 913–33
[41] Hintermüller M, Laurain A and Novotny A A 2012 Second-order topological expansion for electrical impedance tomography *Adv. Comput. Math.* **36** 235–65

[42] Hyvönen N 2009 Approximating idealized boundary data of electric impedance tomography by electrode measurements *Math. Models Methods Appl. Sci.* **19** 1185–202
[43] Hyvönen N, Piiroinen P and Seiskari O 2012 Point measurements for a Neumann-to-Dirichlet map and the Calderón problem in the plane *SIAM J. Math. Anal.* **44** 3526–36
[44] Ikehata M 1999 How to draw a picture of an unknown inclusion from boundary measurements. Two mathematical inversion algorithms *J. Inverse Ill-Posed Probl.* **7** 255–71
[45] Ikehata M and Siltanen S 2000 Numerical method for finding the convex hull of an inclusion in conductivity from boundary measurements *Inverse Problems* **16** 1043–52
[46] Isakov V 2007 On uniqueness in the inverse conductivity problem with local data *Inverse Problems Imaging* **1** 95–105
[47] Kalise D, Kunisch K and Sturm K 2018 Optimal actuator design based on shape calculus *Mathematical Models and Methods in Applied Sciences* **28** 2667–717
[48] Kenig C and Salo M 2014 Recent progress in the Calderón problem with partial data *Inverse Problems and Applications* (Contemporary Mathematics vol 615) (Providence, RI: American Mathematical Society) pp 193–222
[49] Kenig C E, Sjöstrand J and Uhlmann G 2007 The Calderón problem with partial data *Ann. Math.* **165** 567–91
[50] Kirsch A 1998 Characterization of the shape of a scattering obstacle using the spectral data of the far field operator *Inverse Problems* **14** 1489–512
[51] Knudsen K 2006 The Calderón problem with partial data for less smooth conductivities *Commun. PDE* **31** 57–71
[52] Krupchyk K and Uhlmann G 2016 The Calderón problem with partial data for conductivities with 3/2 derivatives *Commun. Math. Phys.* **348** 185–219
[53] Langtangen H and Logg A 2017 *Solving PDEs in Python: The FEniCS Tutorial I* (Simula SpringerBriefs on Computing) (Berlin: Springer International Publishing)
[54] Laurain A and Sturm K 2016 Distributed shape derivative *via* averaged adjoint method and applications *ESAIM: Math. Modelling Numer. Anal.* **50** 1241–67
[55] Logg A, Mardal K-A and Wells G N (eds) 2012 *Automated Solution of Differential Equations by the Finite Element Method* (Lecture Notes in Computational Science and Engineering vol 84) (Berlin: Springer)
[56] Loke M, Chambers J, Rucker D, Kuras O and Wilkinson P 2013 Recent developments in the direct-current geoelectrical imaging method *J. Appl. Geophys.* **95** 135–56
[57] Nicaise S and Sändig A-M 1994 General interface problems. I, II *Math. Methods Appl. Sci.* **17** 431–50
[58] Pridmore D, Hohmann G, Ward S and Sill W 1981 An investigation of finite-element modeling for electrical and electromagnetic data in three dimensions *Geophysics* **46** 1009–24
[59] Revil A, Karaoulis M, Johnson T and Kemna A 2012 Review: some low-frequency electrical methods for subsurface characterization and monitoring in hydrogeology *Hydrogeology Journal* **20** 617–58
[60] Schaa R, Gross L and du Plessis J 2016 PDE-based geophysical modelling using finite elements: examples from 3D resistivity and 2D magnetotellurics *J. Geophys. Eng.* **13** S59–73
[61] Sokołowski J and Zolésio J-P 1992 *Introduction to Shape Optimization: Shape Sensitivity Analysis* (Springer Series in Computational Mathematics vol 16) (Berlin: Springer)
[62] Somersalo E, Cheney M and Isaacson D 1992 Existence and uniqueness for electrode models for electric current computed tomography *SIAM J. Appl. Math.* **52** 1023–40
[63] Sturm K 2014 On shape optimization with non-linear partial differential equations *PhD Thesis* Technische Universität Berlin
[64] Sturm K 2015 Minimax Lagrangian approach to the differentiability of nonlinear pde constrained shape functions without saddle point assumption *SIAM J. Control Optim.* **53** 2017–39
[65] Sturm K 2016 Shape optimization with nonsmooth cost functions: from theory to numerics *SIAM J. Control Optim.* **54** 3319–46
[66] Tröltzsch F 2010 *Optimal Control of Partial Differential Equations: Theory, Methods and Applications* (Graduate Studies in Mathematics vol 112) (Providence, RI: American Mathematical Society) Translated from the 2005 German original by Jürgen Sprekels
[67] Virieux J and Operto S 2009 An overview of full-waveform inversion in exploration geophysics *Geophysics* **74** WCC1–26
[68] Ziemer W P 1989 *Weakly Differentiable Functions* (New York: Springer)